

AMERICAN UNIVERSITY OF BEIRUT

THE PERFORMANCE OF SOLAR-WIND ENERGY
TOWERS USING A LAGRANGIAN-EULERIAN
MULTIPHASE MODEL

by
LINA MOHAMAD HIJAZI

A thesis
submitted in partial fulfillment of the requirements
for the degree of Master of Mechanical Engineering
to the Department of Mechanical Engineering
of the Faculty of Engineering and Architecture
at the American University of Beirut

Beirut, Lebanon
April, 2016

AMERICAN UNIVERSITY OF BEIRUT

THE PERFORMANCE OF SOLAR-WIND ENERGY TOWERS
USING A LAGRANGIAN-EULERIAN MULTIPHASE
MODEL

by
LINA MOHAMAD HIJAZI

Approved by:

Dr. Fadi Moukalled, Professor
Department of Mechanical Engineering

Fadi Moukalled

Advisor

Dr. Marwan Darwish, Professor
Department of Mechanical Engineering

Marwan Darwish

Member of Committee

for _____
Dr. Kamel Ghali, Associate Professor
Department of Mechanical Engineering

Fadi Moukalled

Member of Committee

Date of thesis defense: April 21, 2016

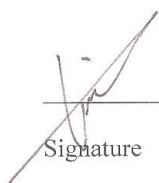
AMERICAN UNIVERSITY OF BEIRUT
THESIS, DISSERTATION, PROJECT RELEASE FORM

Student Name: HIJAZI LINA MOHAMAD
Last First Middle

Master's Thesis Master's Project Doctoral Dissertation

I authorize the American University of Beirut to: (a) reproduce hard or electronic copies of my thesis, dissertation, or project; (b) include such copies in the archives and digital repositories of the University; and (c) make freely available such copies to third parties for research or educational purposes.

I authorize the American University of Beirut, **three years after the date of submitting my thesis, dissertation, or project**, to: (a) reproduce hard or electronic copies of it; (b) include such copies in the archives and digital repositories of the University; and (c) make freely available such copies to third parties for research or educational purposes.

 _____
Signature Date
May 3, 2016

ACKNOWLEDGMENTS

I would like to give a special thanks to my advisor Prof. Fadl Moukalled and my colleague Iyad Faysal (Phd Candidate at the Department of Mechanical Engineering at the American University of Beirut) for their continuous valuable support, help, input and time that allowed the completion of this work.

Thank you as well to my colleagues within the CFD group that provided moral support at all times.

Thank you to the committee members of my research that gave time to give valuable feedback to enhance the scope of this work.

AN ABSTRACT OF THE THESIS OF

Lina Hijazi for Master of Mechanical Engineering

Major: Applied Energy

Title: The Performance of Solar-Wind Energy Towers using a Lagrangian-Eulerian Multiphase Model

State of the art computational fluid dynamics (CFD) techniques have become indispensable for understanding physical phenomena, and for modeling and optimizing the performance of engineering devices involving fluid flow and heat and mass transfer mechanisms. Solar wind energy towers have been recently regarded as a bold new approach to the United States and other nations for their ability to provide clean and sustainable energy, overcoming the burdens of alternative energy sources. An energy tower is a tall tower, at least 400 m high, located in a hot and dry region whereby cool water sprayed at top will evaporate and create a downdraft. The produced high velocity airflow will drive turbines at the bottom of the tower and generate electricity. A 2D numerical model of a prospected tower is constructed to study the impact of different operating parameters including spray droplet diameter, spray flow rate, and ambient conditions on the performance of the tower. A Lagrangian-Eulerian multiphase technique is adopted for simulating droplet transport and evaporation. The model is first validated with published measured data extracted from a small scale PDEC experimental test facility at the Conphoebus Institute in Sicily. Results show that the model is able to accurately predict the evaporation phenomena and that an exit velocity of 33.2m/s can be achieved over a 1000m height tower.

CONTENTS

ACKNOWLEDGEMENTS	v
ABSTRACT.....	vi
LIST OF ILLUSTRATIONS.....	ix
LIST OF TABLES.....	xiii

Chapter

1. INTRODUCTION.....	1
1.1. DESCRIPTION OF THE PROBLEM.....	7
1.2. OBJECTIVES.....	7
2. LAGRANGIAN-EULERIAN MODEL.....	9
2.1. CONTINUOUS PHASE MODEL.....	10
2.2. DISCRETE PHASE MODEL.....	12
2.3. INTERPHASE COUPLING.....	13
2.4. UNDER-RELAXATION OF SOURCE TERMS.....	15
3. TURBULENCE MODELING.....	17
3.1. STANDARD K-E MODEL.....	18
3.2. LAGRANGIAN-EULERIAN TURBULENCE MODEL.....	20
4. NUMERICAL PROCEDURE.....	22
4.1. SOLUTION METHODOLOGY FOR THE CONTINUOUS PHASE.....	22
4.1.1. Mesh Generation (Finite Volume Method).....	22
4.1.2. Discretization of the Diffusion Term.....	22
4.1.3. Discretization of the Convective Term.....	22
4.1.4. Pressure-Velocity Coupling.....	23
4.1.5. Solvers.....	23
4.2. NUMERICAL METHODS FOR THE DISCRETE PHASE.....	24
4.2.1. Solving the Equations of Motion.....	24

5. MODEL DESCRIPTION	26
5.1. PHYSICAL MODEL	26
5.2. MESH INDEPENDENCE	27
5.3. JUDGING CONVERGENCE	28
5.4. BOUNDARY CONDITIONS	28
5.5. USER-DEFINED FUNCTIONS	30
5.5.1. Mixture Density	30
5.5.2. Buoyancy Force	31
5.5.3. Relative Humidity	31
6. EXPERIMENTAL VALIDATION	33
7. RESULTS AND PARAMETRIC ANALYSIS	35
7.1. TEST SERIES I- 20M TOWER	36
7.1.1. Base Case	36
7.1.1.1. Impact of Water Mass Flow Rate	36
7.1.1.2. Impact of Droplet Diameter	46
7.1.1.3. 3D Simulation	49
7.1.2. Impact of Varying Ambient Temperature and Outdoor Relative Humidity	52
7.2. TEST SERIES II- 100M TOWER	56
7.2.1. Impact of Water Mass Flow Rate	57
7.2.2. Impact of Droplet Diameter	59
7.3. TEST SERIES III- 400M TOWER	62
7.3.1. Impact of Water Mass Flow Rate	63
7.3.2. Impact of Droplet Diameter	65
7.3.3. Impact of Tower Height to Diameter Ratio	68
7.4. TEST SERIES V – 1000M TOWER	72
7.4.1. Impact of Water Mass Flow Rate	72
7.4.2. Impact of Droplet Diameter	74
7.5. HIGH LEVEL SUMMARY	78
8. CONCLUSION AND FUTURE WORK	80
REFERENCES	82

ILLUSTRATIONS

Figure	Page
Figure 1. Effect of Under-Relaxing Source Terms on Convergence.....	16
Figure 2. Energy Tower Schematic	26
Figure 3. Energy Tower with Grid Regions	27
Figure 4. Initial Airflow Profile (Without Spray).....	29
Figure 5. Computational Domain with Boundary Conditions.....	30
Figure 6. PDEC Experimental Test Facility	33
Figure 7. Tower 20x8- Base Case- Exit Density vs. Injection Rate	37
Figure 8. Tower 20x8- Base Case- Exit Velocity vs. Injection Rate.....	38
Figure 9. Tower 20x8- Base Case- Exit Temperature vs. Injection Rate	38
Figure 10. Tower 20x8- Base Case- Exit Relative Humidity vs. Injection Rate	39
Figure 11. Tower 20x8- Base Case- Q vs. Injection Rate	39
Figure 12. Tower 20x8- BC- Contour of Density for Injection Rate 0.31kg/s.....	40
Figure 13. Tower 20x8- BC- Contour of Density for Injection Rate 1.26kg/s.....	41
Figure 14. Tower 20x8- BC- Contour of Density for Injection Rate 2.51kg/s.....	41
Figure 15. Tower 20x8- BC- Contour of Temperature for Injection Rate 0.31kg/s.....	42
Figure 16. Tower 20x8- BC- Contour of Temperature for Injection Rate 1.26kg/s.....	42
Figure 17. Tower 20x8- BC- Contour of Temperature for Injection Rate 2.51kg/s.....	43
Figure 18. Tower 20x8- BC- Contour of RH for Injection Rate 0.31kg/s.....	43
Figure 19. Tower 20x8- BC- Contour of RH for Injection Rate 1.26kg/s.....	44
Figure 20. Tower 20x8- BC- Contour of RH for Injection Rate 2.51kg/s.....	44

Figure 21. Tower 20x8-BC- Evolution of Density from Inlet to Outlet vs. Injection Rate	45
Figure 22. Tower 20x8-BC- Evolution of Temperature from Inlet to Outlet vs. Injection Rate.....	46
Figure 23. Tower 20x8-BC- Evolution of RH from Inlet to Outlet vs. Injection Rate...	46
Figure 24. Tower 20x8-BC- Evolution of Density from Inlet to Outlet vs. Droplet Diameter	48
Figure 25. Tower 20x8-BC- Evolution of Temperature from Inlet to Outlet vs. Droplet Diameter	48
Figure 26. Tower 20x8-BC- Evolution of RH from Inlet to Outlet vs. Droplet Diameter	49
Figure 27. 3D Tower (20m).....	50
Figure 28. Average Exit Density (2D vs. 3D)	50
Figure 29. Average Exit Velocity (2D vs. 3D)	51
Figure 30. Average Exit Temperature (2D vs. 3D)	51
Figure 31. Average Exit RH (2D vs. 3D)	52
Figure 32. Tower 20x8- Q vs. Injection Rate	53
Figure 33. Tower 20x8- Density vs. Injection Rate.....	54
Figure 34. Tower 20x8- Velocity vs. Injection Rate	54
Figure 35. Tower 20x8- Temperature vs. Injection Rate.....	55
Figure 36. Tower 20x8- Relative Humidity vs. Injection Rate	55
Figure 37. Tower 20x8- Exit Velocity vs. Temperature	56
Figure 38. Tower 20x8- Exit Velocity vs. Outdoor Relative Humidity	56
Figure 39. Tower 100x40- Q vs. Injection Rate	57
Figure 40. Tower 100x40- Density vs. Injection Rate.....	58
Figure 41. Tower 100x40- Velocity vs. Injection Rate	58

Figure 42. Tower 100x40- Temperature vs. Injection Rate.....	59
Figure 43. Tower 100x40- Relative Humidity vs. Injection Rate	59
Figure 44. Tower 100x40- Q vs. Droplet Diameter.....	60
Figure 45. Tower 100x40- Density vs. Droplet Diameter	61
Figure 46. Tower 100x40- Velocity vs. Droplet Diameter.....	61
Figure 47. Tower 100x40- Temperature vs. Droplet Diameter	62
Figure 48. Tower 100x40- Relative Humidity vs. Droplet Diameter.....	62
Figure 49. Tower 400x160- Q vs. Injection Rate	63
Figure 50. Tower 400x160- Density vs. Injection Rate.....	64
Figure 51. Tower 400x160- Velocity vs. Injection Rate	64
Figure 52. Tower 400x160- Temperature vs. Injection Rate.....	65
Figure 53. Tower 400x160- Relative Humidity vs. Injection Rate	65
Figure 54. Tower 400x160- Q vs. Droplet Diameter.....	66
Figure 55. Tower 400x160- Density vs. Droplet Diameter	66
Figure 56. Tower 400x160- Velocity vs. Droplet Diameter.....	67
Figure 57. Tower 400x160- Temperature vs. Droplet Diameter	67
Figure 58. Tower 400x160- Relative Humidity vs. Droplet Diameter.....	68
Figure 59. Impact of Tower H/D Ratio- Q vs/ Injection Rate	69
Figure 60. Impact of Tower H/D Ratio- Density vs/ Injection Rate.....	70
Figure 61. Impact of Tower H/D Ratio-Velocity vs/ Injection Rate	70
Figure 62. Impact of Tower H/D Ratio-Temperature vs/ Injection Rate.....	71
Figure 63. Impact of Tower H/D Ratio-Relative Humidity vs/ Injection Rate	71
Figure 64. Tower 1000x400- Q vs. Injection Rate	72
Figure 65. Tower 1000x400- Density vs. Injection Rate.....	73

Figure 66. Tower 1000x400- Velocity vs. Injection Rate	73
Figure 67. Tower 1000x400- Temperature vs. Injection Rate.....	74
Figure 68. Tower 1000x400- Relative Humidity vs. Injection Rate	74
Figure 69. Tower 1000x400- Q vs. Droplet Diameter.....	76
Figure 70. Tower 1000x400- Density vs. Droplet Diameter	76
Figure 71. Tower 1000x400- Velocity vs. Droplet Diameter.....	77
Figure 72. Tower 1000x400- Temperature vs. Droplet Diameter	77
Figure 73. Tower 1000x400- Relative Humidity vs. Droplet Diameter.....	78
Figure 74. V99 and Mdot99 vs. Tower Height.....	79

TABLES

Table	Page
Table 1. Discretization Schemes for Discrete Phase Model	24
Table 2. Energy Tower Dimensions	26
Table 3. Tower Mesh Sizes.....	27
Table 4. Microniser Spray System.....	34
Table 5. Comparison between Measured and Predicted Data	34
Table 6. Test Cases Designation and Parameters	36
Table 7. Tower 20x8- Temperature Drop	53
Table 8. Impact of Tower Diameter- Cases	68
Table 9. Droplet Diameter which Induces Largest Temperature Drop	75

Dedication addressed

To my friends & family

CHAPTER 1

INTRODUCTION

A downdraft energy tower is a power plant which produces electricity in hot and dry climates. It is composed of a hollow cylinder with a spraying system at the top and turbines located at the bottom. Water is pumped to the top of the tower and collected by a spraying system. As water is sprayed across the diameter of the shaft, evaporation takes place and the air inside the tower will become denser and cooler than the ambient air thereby creating a downdraft within the enclosed space. The occurring phenomenon is opposite to what happens in a solar chimney. At the bottom of the tower, the high velocity airflow will drive turbines and generate electricity. As cool air descends dry and warmer air is sucked in from the top and the process is reinitiated. The exterior of the tower is composed of vertical wind vanes that capture prevailing winds and tunnel them through a separate channel down to the turbines. The uniqueness of this technology comes with its unlimited capacity to produce energy day and night and its ability to operate at relatively low fuel consumption.

The concept of the energy tower was first introduced by Phillip Carlson in 1975 [1]. He suggested initiating a downdraft in a hollow duct by spraying water at a high altitude and harnessing power from turbines located at the outlet. However, there were many shortcomings in Carlson's patent, which were tackled by Zaslavsky [2]. Carlson defined the cooling potential of the tower solely by the amount of evaporated water needed to bring down the temperature to saturated conditions. In fact, he did not take into account the potential cooling over the height of the tower. Zaslavsky argued that the air outside the tower follows a dry adiabatic process where air is warmed to

compression by 1°C for every 100m in elevation. However, the air inside the tower is theoretically cooled to saturation almost instantaneously and as the air descends, it is warmed by 0.5°C for every 100m in elevation, following a wet adiabatic process. In fact, the cooling process takes place gradually rather than immediately and as air falls inside the shaft, it can be further cooled by evaporation, keeping the air temperature close to the wet adiabatic temperature. For the turbines to generate an effective amount of power there should be a large pressure difference between the air inside the tower and the air outside. This is achieved by having a tower with significant height and ensuring that further humidification and cooling is achieved along the tower. Therefore, excess water discharge is favorable and the excess water that is not initially evaporated will be available for evaporation as the air descends. Liquid droplets will transmit momentum and gravitational energy to the air inside the shaft, which will further enhance the power capabilities of the tower.

Convective downdrafts have been significant in studying rainfalls, microbursts, wind shear, and thunderstorms. This phenomenon has been extensively studied over the past few decades in the aviation industry to detect the danger caused by wind shear on airplanes. Downdrafts are typically caused by evaporation, precipitation loading, and pressure forces. In an energy tower the downdraft is contained inside a hollow shaft. As droplets evaporate, the denser air accelerates downwards, and therefore increasing the negative available potential energy. Technically, it is the energy required to overcome the negatively buoyant energy the environment exerts on an air particle. Precipitation loading, on the other hand, is defined by the amount of water vapor (kg) mixed per kg of air. Both phenomena enhance the downdraft velocity, but precipitation loading alone cannot initiate a

downdraft. Evaporation enhances the pressure gradient, whereas unevaporated water is considered an additional source of energy, where both contribute to enhancing the vertical downdraft. In the case of evaporation, the negative available potential energy increases because the air becomes cooler (denser) than the surrounding air causing it to accelerate downwards.

The maximum net power does not only depend on the amount of water to be sprayed, but also on the size of the droplets. Carlson suggested decreasing droplet diameter as much as possible in order to ensure instantaneous evaporation. In return, Zaslavsky argued that decreasing the droplet diameter will increase the spraying energy requirement and will also pose a problem in the accumulation of precipitated salt residuals on equipment, which will make it difficult to remove.

When there is a high concentration of water exiting the spraying system, there is a possibility for droplets to collide. Depending on the efficiency of collision, and the effectiveness of intermolecular forces, two droplets may coalesce to form one bigger droplet. Since water has a relatively large surface tension, there is a good chance that droplets that collide will coalesce since the stronger the surface tension, the stronger are the intermolecular forces. On the other hand, droplets that do not coalesce will bounce away from each other [3]. Hassid et al. [4] studied the effects of coalescence in an energy tower using models described by O'Rourke (1981) and O'Rourke and Anthony (1987). The results show that coalescence is substantial in the tower but not important at the top of the tower since the temperature quickly decreases to the wet bulb temperature. However, droplets increase in size as they move down, which will result in the deviation of the temperature profile from the wet adiabatic line and

therefore a decrease in the specific potential energy. This energy is either transformed to frictional losses or to shaft power by the turbines.

Computational Fluid Dynamics has been a popular approach to modeling and understanding the main physical phenomena occurring within energy towers. This is mainly due to the fact that capturing experimental data is expensive and time consuming. In order to simulate droplet transport and evaporation, two approaches can be adopted, the first being the Lagrangian method and the other being the Eulerian Method. In all cases, the gaseous phase is represented in a Eulerian framework where the Navier Stokes equations are solved. In the Eulerian-Eulerian (EE) approach, each phase is treated in a Eulerian Framework. Multiple phases are treated separately yet interactively. Both the spray and gaseous phase are solved in the same numerical procedure where the Navier Stokes equations are extended to incorporate interphase exchange coefficients which represent the transfer of mass, momentum and energy from one phase to the other. A multiphase model can be used in FLUENT to treat EE methods. In the Lagrangian-Eulerian (LE) approach, the droplets are represented in the discrete phase, whereas the gas phase is represented in the continuous phase. The solutions are fully coupled since both phases impact each other. Interphase exchange coefficients of mass, momentum, and energy appear in the Eulerian conversation equations and these coefficients are obtained by alternating iterations between equations representing both phases. Achieving numerical convergence is crucial for the success of the LE approach. A discrete phase model in fluent is used to treat LE methods. Subramaniam [5] highlights the superiority of the LE method over the EE Method in capturing and accurately simulating the evaporation process. In fact, the

majority of CFD studies in literature involving fluid flow and evaporation adopted the LE approach.

A similar principle to the energy tower has been used in evaporative cooling towers. These towers, commonly known as passive downdraft evaporative cooling towers (PDEC), are just a few stories high with the aim of cooling and ventilating spaces rather than generating electricity. Typically, they are composed of a wind catcher, shaft, and an evaporative device such as a wetted pad or spray. D. Kang and R. K. Strand [6] followed a Lagrangian-Eulerian Approach and developed a two dimensional, steady state model under turbulent flow conditions in order to understand and explain the main phenomena occurring within the tower. The model was simulated using FLUENT. A parametric study was performed to investigate the impact of varying droplet size, outdoor relative humidity and ambient wind speed. Results show that with a low spray flow rate, 50L/hr, no significant change in temperature was observed at variable relative humidity and wind speed. Whereas, upon varying droplet size from 50 microns to 300 microns the highest temperature drop was observed for a droplet size of 100 microns. However, the exit velocity was not impacted by droplet diameter. A similar approach to evaluating the cooling performance of a PDEC tower was conducted by V. Kalantar [7], except the model was three dimensional. He additionally developed a general purpose mathematical model in c++, applicable to several tower geometries, based on wind velocity and temperature data measured both at the inlet and outlet which were acquired over a period of four days. The model is able to predict air conditions at the exit of the tower. M.J. Cook et al. [8] also used CFD to model airflows in PDEC towers but used CFX instead of FLUENT. The objective was to predict conditions at the exit of the tower by understanding the way

liquid particles interact with the gaseous phase. The injection rate was calibrated by means of a sensitivity analysis to suit target conditions at the outlet.

The traditional energy tower heights between 600m to 1200m and will have a diameter ranging from 100m to 400m [4]. External environmental conditions such as temperature, pressure, and relative humidity, vary with height. Such parameters must be evaluated properly upon modeling ambient conditions. E. Omer et al. [9] devised an optimization algorithm which can simultaneously find optimal pipe diameter (mm), discharge rate (m^3/s), and pump power (MW) given a tower height, diameter, distance from sea, and initial investment. The mathematical model takes into account climate data in an area near the red sea. The temperature was extrapolated to a height of 1,280m, which is the height of the tower, from data available at a height of 900m whereas the humidity ratio was assumed to be constant. For each month, there was one representative value for temperature and one for humidity ratio. Results show that for each month of the year there is an optimum discharge rate that will maximize net power output. G. Abhinava et al. [10] studied the intensity of downdrafts in a 500m energy tower. The final output velocity was calculated by squaring the sum of negative available potential energy, precipitation loading, and maximum horizontal momentum equations. It was shown that the power producing capabilities of the tower increase with tower height and swept area of the turbines. At the same time, the final output velocity is related to the cooling potential within the tower. Meaning that as the difference in temperature between the internal environment and ambient conditions increase, the output velocity increases.

The objective of this research is to conduct a parametric study on a solar wind energy tower using a LE method. The tower will be 2D and simulated in steady state

using ANSYS Fluent 14.5. The research differs from what has been previously reported in literature in a sense that the true performance of the tower is analyzed independent of geometry manipulation. A full-buoyancy model is adopted and incorporated as a user-defined function, which expresses the buoyancy driven flow in terms of density difference and is then added as a source term in the momentum equation. In addition, the quantity of mass that can be produced in comparison to the amount of water that is sprayed is investigated. The model also predicts conditions at the exit of the tower, such as velocity, temperature, density, and relative humidity under various ambient conditions and spray characteristics.

1.1. Description of the problem

In order to better understand the behavior of downdrafts in an energy tower independent of geometry manipulation, a two dimensional axisymmetric model has been developed. The tower will be simulated using the using the discrete phase model in ANSYS FLUENT 14.5 under a Lagrangian-Eulerian framework, where the fluid is treated in the continuous phase, whereas the liquid droplets are treated in the discrete phase.

1.2. Objectives

The objective of this project is to model simultaneous heat and mass transfer within an energy tower under various ambient conditions and spray characteristics. The CFD model will enable us to understand the main physical phenomena occurring within the tower as well as predict the exit conditions at the outlet. In addition, the

project addresses speculation on whether this invention will actually work and proves that theory of operation does not contradict laws of thermodynamics. The computational domain selected is a hollow cylindrical column where exit conditions are reported and therefore assessing performance prior to geometry manipulation at the exit where a cone exists at the center of the base to divert the airflow to channels where the wind turbines are located.

CHAPTER 2

LAGRANGIAN-EULERIAN MODEL

In FLUENT, the discrete phase model follows a Lagrangian - Eulerian approach. The fluid flow is treated in the continuous phase by solving the time-averaged Navier-Stokes equations, while the discrete phase is solved by tracking droplets in the flow field. The discrete phase can exchange mass, momentum and energy with the continuous phase and this is modeled by the inclusion of source terms from the discrete phase into the continuous phase equations. The downdraft model consists of equations of heat and mass transfer, turbulence, and species. The sets of equations in the continuous phase solve equations of conservation of mass, momentum, energy and species transport whereas equations for the discrete phase calculate the trajectory of water droplets. Both phases are highly interactive, and the two way coupling procedure is solved in FLUENT as follows:

1. Initialize flow field by solving the continuous phase
2. Calculate the discrete phase particle trajectory and obtain interphase exchange coefficients
3. Calculate the continuous phase with the inclusion of interphase exchange coefficients adopted from the discrete phase
4. Calculate discrete phase in the modified flow field
5. Repeat 2-4 until a converged solution is achieved

The next sections will describe models of continuous phase, discrete phase, turbulence, and coupling between phases.

The model undertakes the following assumptions:

- Simulation is conducted in steady state
- 2D Axi-symmetric
- The flow is fully turbulent
- The spray is dilute
- The droplets retain a spherical shape
- The droplet in the discrete phase is composed of a single species, liquid water
- The continuous phase is the gas phase containing two species, air and water vapor
- The wall has zero flux, therefore any backflow current is neglected
- The evaporation process is gradual, slow, and convection-diffusion controlled
- Latent heat variation with droplet temperature is negligible

2.1. Continuous Phase Model

In solving the continuous phase, equations of conservation of mass, momentum, energy and species are solved. In the beginning of the simulation, the flow field is initialized by solving the equations while excluding the interphase exchange coefficients. After the discrete phase equations are solved and the source terms are obtained, then the continuous phase equations are solved with the inclusion of the source terms.

The equation for conservation of mass is:

$$\frac{\partial \rho}{\partial t} + \nabla \cdot (\rho \mathbf{v}) = S_m \quad (1)$$

Where ρ is the density of air (kg/m^3), \mathbf{v} is the air velocity (m/s) and S_m is the addition of mass from the discrete phase ($\text{kg/m}^3\text{s}$).

The momentum equation is expressed as follows:

$$\frac{\partial(\rho\mathbf{v})}{\partial t} + \nabla \cdot (\rho\mathbf{v}\mathbf{v}) = \nabla \cdot (\bar{\boldsymbol{\tau}}) + \rho\mathbf{g} - \nabla p + \mathbf{F}_m \quad (2)$$

$$\bar{\boldsymbol{\tau}} = \mu \left[(\nabla\mathbf{v} + \nabla\mathbf{v}^T) - \frac{2}{3}\nabla \cdot \mathbf{v}\mathbf{I} \right] \quad (3)$$

Where μ is the molecular viscosity ($\text{kg/m}\cdot\text{s}^2$), \mathbf{g} is the gravitational acceleration (m/s^2), $\bar{\boldsymbol{\tau}}$ is the stress tensor, p is the static pressure (Pa), \mathbf{I} is the unit tensor, and \mathbf{F}_m is the momentum source from the discrete phase ($\text{kg/m}^2\text{s}^2$).

The Energy equation is expressed in terms of internal energy as follows:

$$\frac{\partial}{\partial t}(\rho E) + \nabla \cdot (\rho\mathbf{v}E) = -p\nabla\mathbf{v} + \nabla \cdot (k\nabla T) - \nabla \cdot \left(\sum_j h_j \mathbf{J}_j \right) + \Phi + S_h \quad (4)$$

Where E is the internal energy (J/kg), k is the effective thermal conductivity ($\text{W/m}\cdot\text{K}$), T is the air temperature (K), h is the enthalpy of species j , \mathbf{J} is the diffusion flux of species j ($\text{kg/m}^2\cdot\text{s}$), Φ is the Rayleigh Dissipation Function ($\text{kg/s}^3\cdot\text{m}$), and S_h is the heat source from the discrete phase

The term $\nabla \cdot (\sum_j h_j \mathbf{J}_j)$ expresses the transport of enthalpy due to species diffusion. If the Lewis Number, defined by the ratio of thermal diffusivity to mass diffusivity is unity, then this term can be neglected for simplicity of calculation. In

liquid/gas simultaneous heat and mass transfer problems, the Lewis number is not always unity. In fact, the influence is directly related to the ambient temperature at the inlet of the tower. The higher the outdoor temperature, the less is the impact of the Lewis number and the profiles of temperature and species concentration are most likely to coincide [11]. In this problem, the potential impacts of the Lewis number on tower performance will not be neglected.

The conservation equation for species transport is shown next. The equation will solve for the local mass fraction m of each species j . In this case, only one species, water vapor, is considered.

$$\frac{\partial}{\partial t}(\rho m_j) + \nabla \cdot (\rho \mathbf{v} m_j) = -\nabla \cdot \mathbf{J}_j + S_m \quad (5)$$

The Mass Diffusion under turbulent flow conditions is expressed as:

$$\mathbf{J}_j = -\left(\rho D_{j,m} + \frac{\mu_t}{Sc_t}\right) \nabla m_j \quad (6)$$

Where μ_t is the turbulent viscosity, $D_{j,m}$ is the diffusion coefficient for species j and Sc is the Schmidt Number taken to be 0.7 by default.

2.2. Discrete Phase Model

In the discrete phase model, the velocity of particles at each point along the trajectory is calculated by stepwise integrating the force balance acting on the particles over the discrete phase time step.

$$\frac{\partial \mathbf{v}_p}{\partial t} = F_D(\mathbf{v} - \mathbf{v}_p) + \mathbf{g} \frac{(\rho_p - \rho)}{\rho_p} + \mathbf{F} \quad (7)$$

The terms \mathbf{v}_p and ρ_p represent the particle velocity and density respectively. The first term on the right hand side of the equation is the Drag force per unit mass of particle. The second term is due to the force of gravity acting on density variation, by which a flow is induced. Finally, \mathbf{F} is the additional acceleration acting on the particle.

The trajectory of the particle is calculated using

$$\frac{dx}{dt} = \mathbf{v}_p \quad (8)$$

F_D can be found by the following expression

$$F_D = \frac{18\mu C_D Re}{24\rho_p d_p^2} \quad (9)$$

Where d_p^2 is the droplet diameter and C_D is the drag coefficient. Since the droplet is assumed to retain a spherical shape, the calculation of the drag coefficient follows Eq. 10 and the coefficients are obtained from the works of Morsi and Alexander

$$C_D = a_1 + \frac{a_2}{Re} + \frac{a_3}{Re^2} \quad (10)$$

2.3. Interphase Coupling

After calculating the trajectory of the particles, the source terms can be found by a coupling scheme. The source terms link the exchange of mass, momentum, and energy gained from the discrete phase into the continuous phase.

The addition of mass from the discrete phase is computed by evaluating the exchange of mass from one control volume to the next

$$S_m = \frac{\Delta m_p}{m_{p,0}} \dot{m}_{p,0} \quad (11)$$

Similarly, the exchange of momentum between control volumes will appear in the momentum equation source term F_m and is calculated as such:

$$F_m = \sum (F_D(\mathbf{v}_p - \mathbf{v}) + F_{additional}) \dot{m}_p \Delta t \quad (12)$$

Where \dot{m}_p is the particle mass flow rate, and Δt is the time step

The vaporization process of a droplet is governed by Law 2 in FLUENT and follows a convection diffusion controlled model. The rate of droplet mass change is governed by Eq. (13)

$$\frac{dm_p}{dt} = k_c A_p \rho_\infty \ln(1 + B_m) \quad (13)$$

Where k_c is the mass transfer coefficient (m/s), A_p is the droplet surface area (m^2), ρ_∞ is the density of the bulk gas (kg/m^3), and B_m is the spalding mass number

k_c can be calculated from the Sherwood number correlation function

$$Sh = \frac{k_c d_p}{D_{i,m}} = 2 + 0.6 Re^{0.5} Sc^{\frac{1}{3}} \quad (14)$$

The spalding mass number is defined by:

$$B_m = \frac{Y_{j,s} - Y_{j,\infty}}{1 - Y_{j,s}} \quad (15)$$

Where $Y_{j,s}$ is the vapor mass fraction at the surface, and $Y_{j,\infty}$ is the vapor mass fraction in the bulk gas.

Finally, the volumetric heat source S_h , which is the interphase exchange coefficient appearing in the energy equation represents the heat transfer from the discrete phase to the continuous phase as a particle passes through each control volume

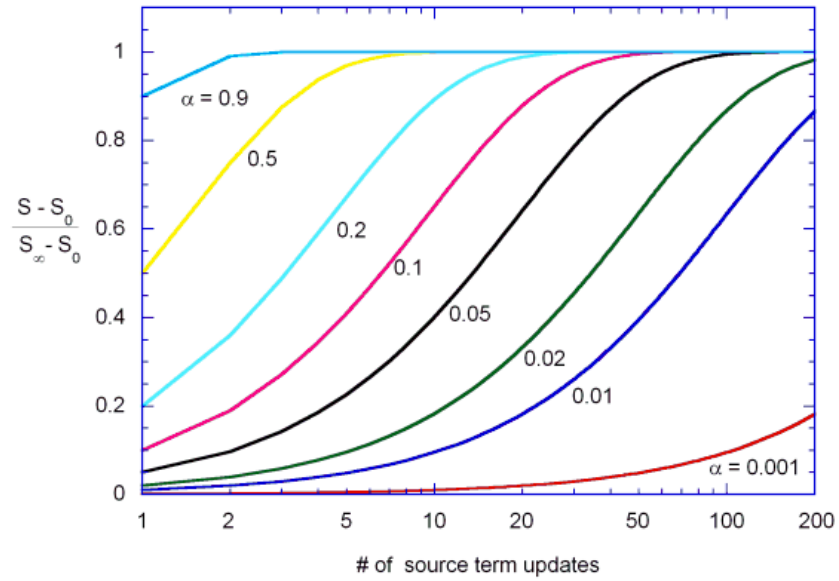
$$S_h = \left[\frac{\overline{m}_p}{m_{p,0}} c_p \Delta T_p + \frac{\Delta m_p}{m_{p,0}} \left(-h_{fg} + \int_{T_{ref}}^{T_p} c_{p,i} dT \right) \right] \dot{m}_{p,0} \quad (16)$$

Where \overline{m}_p is the average mass of the particle in a control volume (kg), $m_{p,0}$ is the initial mass of the particle (kg), Δm_p is the difference between the mass of the particle at the input of a control volume and the mass at the exit of a control volume (kg), c_p is the specific heat of the particle (J/kg.K), h_{fg} is the latent heat (J/kg), $c_{p,i}$ is the specific heat of air (J/kg.K), T_{ref} is the reference temperature for enthalpy, T_p is the temperature of the particle upon exiting the control volume, and $\dot{m}_{p,0}$ is the initial mass flow rate of the particle (kg/s).

2.4. Under-relaxation of Source Terms

In order to increase the stability of the interphase phenomena, the source terms are under-relaxed by a factor α . The source terms are calculated every discrete phase iteration, and for every continuous phase iteration the source terms are under-relaxed by α . The number of continuous phase iterations per discrete phase iteration is determined by α according to the diagram obtained from FLUENT shown in figure 1 below

Figure 1. Effect of Under-Relaxing Source Terms on Convergence



As the number of continuous phase iterations per discrete phase iterations increases, the solution will be more stable but it will take a longer time to converge. In this problem we will take α to be 0.1 and therefore perform 50 continuous phase iterations per 1 discrete phase iteration.

For every continuous phase iteration the source terms are updated as follows

$$S_{m_new} = S_{m_old} + \alpha(S_m - S_{m_old}) \quad (17)$$

$$F_{m_new} = F_{m_old} + \alpha(F_m - F_{m_old}) \quad (18)$$

$$S_{h_new} = S_{h_old} + \alpha(S_h - S_{h_old}) \quad (19)$$

CHAPTER 3

TURBULENCE MODELING

The most popular approach to modelling turbulent flows is the RANS (Reynolds averaged Navier Stokes Equations) method, whereby the flow components are modelled by the sum of an averaged component and a fluctuating component.

$$\phi(x, t) = \overline{\phi(x, t)} + \phi'(x, t) \quad (20)$$

Where ϕ is an instantaneous transport property, such as velocity, temperature, pressure, density, etc.. and x and t are the respective position and time components of the property. The average component $\overline{\phi}$ is obtained from the solution of the Eulerian equations, whereas the fluctuating component ϕ' is modelled. In incompressible flows, the newly developed velocity, pressure and temperature components which take the form of Eq. (20) are replaced into the continuity momentum and energy equations. After averaging techniques a Reynolds stress tensor appears on the right hand side of the momentum equation which is given by τ_R and a turbulent thermal flux appears in the energy equation, given by q_R . The calculation of these stresses, most commonly known as Reynolds stresses, is turbulence modelling.

$$\tau_R = -\rho \overline{v'v'} = \mu_t \{ \nabla v + (\nabla v)^T \} - \frac{2}{3} \rho k I \quad (21)$$

Where μ_t is the turbulent eddy viscosity, and k is the turbulent kinetic energy.

$$q_R = -\rho c_p \overline{v'T'} = k_t \nabla T \quad (22)$$

Where k_t is the turbulent thermal diffusivity.

The problem is therefore reduced to calculating the turbulent eddy viscosity, turbulent kinetic energy and turbulent thermal diffusivity.

3.1. Standard k- ε Model

The most popular approach to modeling turbulent flows in the continuous phase regime is the k - ε model whereby the rate of production of turbulent kinetic energy k and its dissipation rate ε are solved for. The Reynolds stresses are then computed (Eq.21 and 22). The turbulent eddy viscosity and thermal diffusivity are represented as follows

$$\mu_t = \rho C_\mu \frac{k^2}{\varepsilon} \quad (23)$$

Where $C_\mu = 0.09$

$$k_t = \frac{c_p \mu_t}{Pr_t} \quad (24)$$

Where $Pr_t = 0.9$

The k - ε system of equations is

$$\frac{\partial}{\partial t}(\rho k) + \nabla \cdot (\rho v k) = \nabla \cdot (\mu_{eff,k} \nabla k) + P_k + P_b - \rho \varepsilon \quad (25)$$

Where P_k is the production of turbulent kinetic energy due to a mean velocity gradient.

$$P_k = \tau_R : \nabla v \quad (26)$$

Since there exists a simultaneous temperature gradient and gravitational force, we must account for P_b which is the production of turbulent kinetic energy due to buoyancy.

$$\frac{\partial}{\partial t}(\rho\varepsilon) + \nabla \cdot (\rho v\varepsilon) = \nabla \cdot (\mu_{eff,\varepsilon} \nabla \varepsilon) + C_{\varepsilon 1} \frac{\varepsilon}{k} P_k + C_{\varepsilon 3} C_{\varepsilon 1} P_b - C_{\varepsilon 2} \rho \frac{\varepsilon^2}{k} \quad (27)$$

Where $C_{\varepsilon 1} = 1.44$, $C_{\varepsilon 2} = 1.92$

$$C_{\varepsilon 3} = \tanh \left| \frac{v_y}{v_x} \right| \quad (28)$$

v_y is the velocity component in the direction of the gravitational field. If the flow is aligned with the gravitational field, $C_{\varepsilon 3}$ is 1. v_x is the velocity component perpendicular to the direction of the gravitational field. If the flow is perpendicular to the gravitational field, $C_{\varepsilon 3}$ is 0 [13].

$$\mu_{eff,k} = \mu + \frac{\mu_t}{\sigma_k} \quad (29)$$

Where $\sigma_k = 1$

$$\mu_{eff,\varepsilon} = \mu + \frac{\mu_t}{\sigma_\varepsilon} \quad (30)$$

Where $\sigma_\varepsilon = 1.3$

Note that σ is the turbulent Prandtl Number.

3.2. Lagrangian-Eulerian Turbulence Model

In the Lagrangian reference frame, the dispersion of particles due to turbulence can be evaluated by means of a stochastic tracking model, or a particle could model. The trajectory of particles are exposed to turbulent fluctuations such that

$$v_p = \bar{v}_p + v'_p \quad (31)$$

Eq. (31) is replaced in the discrete phase model trajectory equation (Eq.7). In this way, the impact of turbulence on particle dispersion is included. The Discrete Random Walk Model (DRWM), under the umbrella of stochastic tracking is used to model the fluctuating velocity component. This component is sampled by a Gaussian probability distribution function, whereby

$$v'_p = \xi \sqrt{v_p'^2} \quad (32)$$

ξ is a normally distributed random number, and $\sqrt{u_p'^2}$ is the local RMS value of velocity fluctuations. Since a k - ε model is implemented in the continuous phase, we can represent this term as such:

$$\sqrt{v_p'^2} = \sqrt{\frac{2k}{3}} \quad (33)$$

Each eddy is also represented by a characteristic lifetime τ_e

$$\tau_e = 2T_L \quad (34)$$

Where T_L is the lagrangian time scale. For a k - ε model, this time scale can be approximated by:

$$T_L \approx 0.15 \frac{k}{\varepsilon} \tag{35}$$

CHAPTER 4

NUMERICAL PROCEDURE

In order to solve a CFD problem, the space is first discretized (spatial discretization) into a finite number of volumes (commonly known as control volumes). The domain equations are then discretized and solved by numerical methods.

4.1. Solution Methodology for the Continuous Phase

4.1.1. Mesh Generation (Finite Volume Method)

The numerical solution is evaluated in fluent using the finite volume method. The flow field governing equations are converted to algebraic equations and evaluated at each control volume. The flow field properties are stored at the center of each control volume, therefore interpolation techniques are required to find the values at the faces of each control volume.

4.1.2. Discretization of the Diffusion Term

The diffusion term is central-differenced and second order accurate.

4.1.3. Discretization of the Convective Term

As for discretization of the convection term, FLUENT allows to choose between several schemes such as First Order Upwind (FOU), Second Order Upwind (SOU), power law and QUICK. A SOU scheme will be selected for the momentum, energy, species and turbulence equations [6].

4.1.4. Pressure-Velocity Coupling

In solving the Navier-Stokes equation, a pressure term appears in the momentum equation which is used to compute the velocity field, yet this velocity field does not necessarily satisfy conservation of mass. A pressure-velocity coupling model is implemented as a calculation procedure for the Navier-Stokes equations whereby a pressure correction is applied that updates the velocity field to ensure conservation of mass in the continuity equation. A SIMPLE algorithm is selected for this task, and in order to compute the face pressure, a second order scheme is selected.

4.1.5. Solvers

A pressure based segregated solver is imposed on the domain, where pressure correction and momentum equations are initially solved successively.

The segregated Solver will compute the flow field as follows:

1. Solve U-Momentum
2. Solve V-Momentum
3. Solve W-Momentum
4. Solve Continuity (Pressure Correction) equation
5. Update Pressure Field and correct Face Mass Flow Rates, and Cell Velocities.
6. Solve Energy Equation
7. Solve Species
8. Solve Turbulence Equations

If the solution is not converged, then the variables (density, pressure, velocity, etc..) are under-relaxed by α , and the process repeats (1-8).

4.2. Numerical Methods for the Discrete Phase

4.2.1. Solving the Equations of Motion

S. Shukla et al. [12] discussed numerical schemes for the discrete phase model in FLUENT. According to [12], the general equation of motion for a particle can be expressed as

$$\frac{\partial v_p}{\partial t} = \frac{18 \mu}{\rho_p d_p^2} (v - v_p) + a \quad (36)$$

Where a is the acceleration due to all forces except drag.

Eq. (8) and (36) are the domain governing ordinary differential equations which can be solved either by analytical integration or analytical discretization. Four discretization schemes are available in FLUENT, two of which are low order, and two of which are high order. Table 1 below summarizes the available discretization schemes.

Table 1. Discretization Schemes for Discrete Phase Model

Low Order Schemes	High Order Schemes
Implicit	Semi Implicit Trapezoidal
Analytic	Runge-Kutta

It is possible to select a low order scheme, a high order scheme, or a combination of a low order scheme with a high order one. A Semi-Implicit Trapezoidal scheme will give the most accurate results [12], and will therefore be adopted to solve Eq.(36). The discretization is shown below, where n signifies location.

$$\frac{v_p^{n+1} - v_p^n}{\Delta t} = \frac{18 \mu}{\rho_p d_p^2} (v^* - v_p^*) + a^n \quad (37)$$

Where v^* and v_p^* are the average fluid and particle velocities respectively, and computed as shown below

$$v^* = \frac{1}{2} [v^n + v^{n+1}] = \frac{1}{2} [v^n + (v^n + \Delta t \times v_p^n)] \quad (38)$$

$$v_p^* = \frac{1}{2} (v_p^n + v_p^{n+1}) \quad (39)$$

After manipulation, the particle velocity at the new location is computed as follows:

$$v_p^{n+1} = \frac{v_p^n \left(1 - \frac{1}{2} \frac{18 \mu}{\rho_p d_p^2} \Delta t\right) + \frac{18 \mu}{\rho_p d_p^2} \Delta t \left(v^n + \frac{1}{2} \Delta t v_p^n \times \Delta v^n\right) + \Delta t \times a}{1 + \frac{1}{2} \frac{18 \mu}{\rho_p d_p^2} \Delta t} \quad (40)$$

Note that Δv^n is the fluid velocity at the new location. The new particle location is found by trapezoidal discretization of Eq.(8)

$$X_p^{n+1} = X_p^n + \frac{1}{2} \Delta t (v_p^n + v_p^{n+1}) \quad (41)$$

CHAPTER 5

MODEL DESCRIPTION

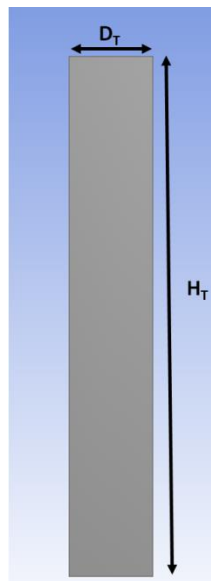
5.1. Physical Model

The Energy Tower under study is a hollow cylinder with a height to diameter ratio of 2.5. According to Zaslavsky [2], the optimal height to diameter ratio for a fixed heighted tower is 2-2.5, therefore the selected ratio falls within the recommended range. Four basic geometry configurations are studied, as displayed in Table 2 below:

Table 2. Energy Tower Dimensions

Number	Height, H_T (m)	Diameter, $2 \times D_T$ (m)
1	20	8
2	100	40
3	400	160
4	1000	400

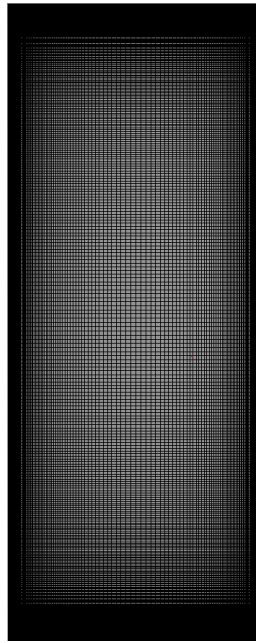
Figure 2. Energy Tower Schematic



5.2. Mesh Independence

A mapped face meshing technique was imposed where the computational domain was discretized into quadrilaterals. A biasing technique was adopted onto the edges to ensure near wall refinement.

Figure 3. Energy Tower with Grid Regions



For each of the four tower configurations displayed in (5.1), a mesh independent test revealed no significant change in results with any further grid refinement. Table 3 below shows the mesh size selected for each configuration.

Table 3. Tower Mesh Sizes

Height, H_T (m)	Diameter, $2x D_T$ (m)	Number of Elements
20	8	64,000
100	40	100,000
400	160	400,000
1000	400	625,000

5.3. Judging Convergence

Several criteria were taken into account for judging convergence. The first criteria is monitoring of scaled residuals. The convergence criteria for continuity, k and ϵ was 10^{-3} , for Velocity components and Species 10^{-5} and for Energy 10^{-6} .

The second criterion is monitoring the net mass flow rate between inlet and outlet. The value must be less than 5 orders of magnitude around zero.

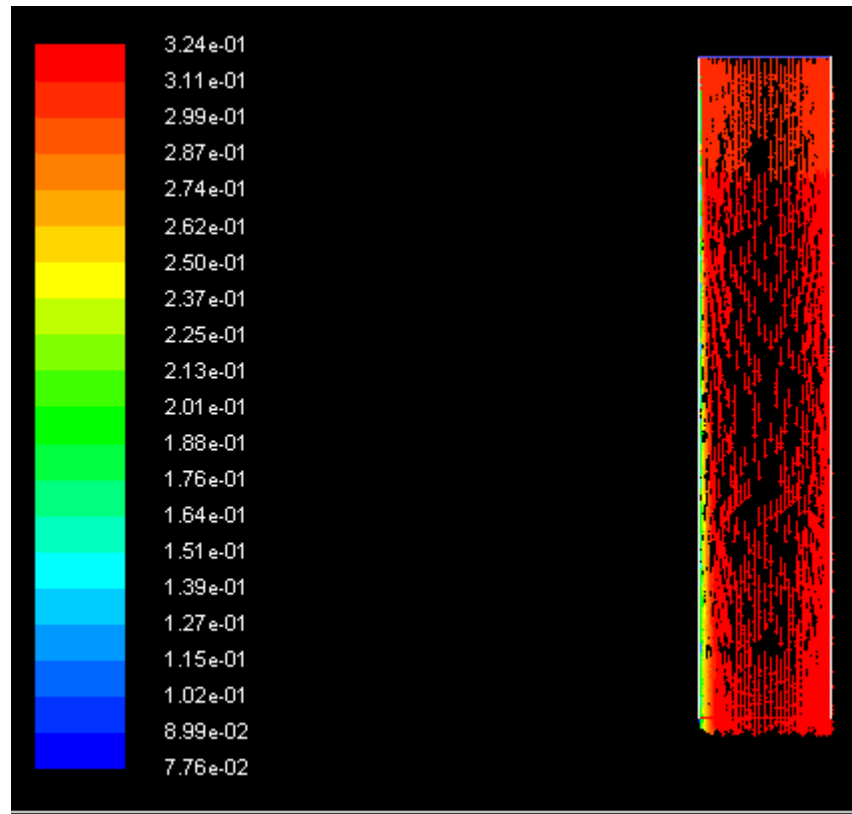
Finally the mass weighted average at outlet for temperature and velocity where monitored. When the value no longer changes, convergence is achieved.

5.4. Boundary Conditions

In this study, a pressure-inlet pressure-outlet boundary condition was imposed on the domain in order to predict the quantity of flow that can potentially be entrained from the environment.

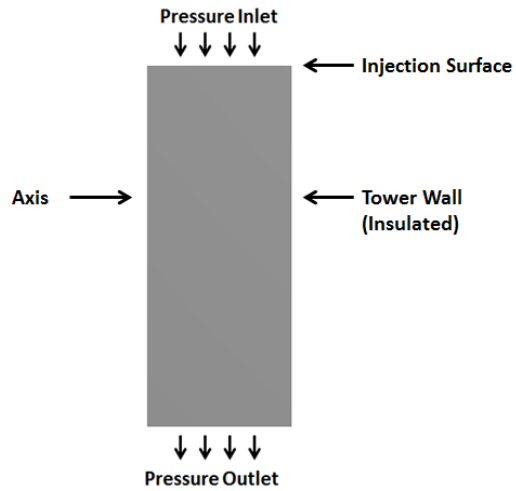
The total pressure selected at the inlet is the lowest value that ensures that no initial reverse flow is occurring in the tower. The total pressure at the inlet represents the summation of both static and dynamic pressure. Pressure at the outlet is set to zero and is interpreted in FLUENT as atmospheric pressure, assigned as 101325Pa. Figure 4 below shows the initial airflow profile prior to spraying any water.

Figure 4. Initial Airflow Profile (Without Spray)



A 2D Axisymmetric Model is implemented, where one edge is assumed to be a fully insulated wall so that external environmental conditions do not influence the flow field within the tower and the second edge is modelled as an axis.

Figure 5. Computational Domain with Boundary Conditions



Water is set to be released from the inlet following a surface injection technique. The spray system is set to be scaled according to face area so that water is uniformly distributed along the inlet. For all cases, water is sprayed at a temperature of 290K.

5.5. User-Defined Functions

5.5.1. Mixture Density

The density of dry air (kg/m^3) is calculated using the incompressible ideal gas law

$$\rho_{dry\ air} = \frac{P \times M_w}{R \times T_{cell}} \quad (42)$$

Where P is the sum of operating pressure 101325Pa and Pressure at each cell, M_w is the Molar Mass of air 28.966 kg/mol, and R is the gas constant 8.3144598 J/mol.K. T_{cell} is the temperature at each cell.

The density of the mixture is computed from a relation given dry air density and species mass fraction (kg/kg) computed at each cell.

$$\rho_{mixture} = \rho_{dry\ air} \frac{1 + W_{water\ vapor}}{1 + 0.609 \times W_{water\ vapor}} \quad (43)$$

5.5.2. Buoyancy Force

The Buoyancy Force (N) due to density difference is computed and added as a source term in the momentum equation.

$$\rho_{ref} = \frac{P \times M_w}{R \times T_{ref}} \quad (44)$$

Where T_{ref} is the ambient air temperature (K).

$$F_{buoyancy} = g(\rho_{mixture} - \rho_{ref}) \quad (45)$$

5.5.3. Relative Humidity

Relative Humidity is computed as a function of humidity ratio W (kg/kg) and dry bulb temperature (K) [14].

$$Relative\ Humidity = \frac{p_w}{p_{ws}} \times 100 \quad (46)$$

Where p_w is the partial pressure of water vapor (Pa)

$$p_w = \frac{P \times W}{W + 0.62198} \quad (47)$$

And p_{ws} is the saturation pressure (Pa)

$$p_{ws} = \exp\left(\frac{C_8}{T} + C_9 + C_{10} \times T + C_{11} \times T^2 + C_{12} \times T^3 + C_{13} \ln T\right) \quad (48)$$

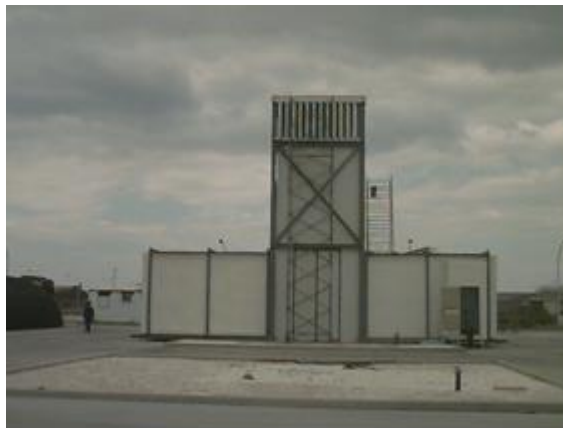
CHAPTER 6

EXPERIMENTAL VALIDATION

The model was validated against full-scale published measured data from a PDEC test facility located in Catania, Sicily at Conphoebus Institute and reported in (kang). The facility is composed of a Tower with dimensions 4.1m x 4.4m x 10.7 m , a wind catcher at the top, and two rooms connected at the north and south sides of the tower each 6m x 3.6m x 4m.

The wind catcher is composed of a metallic structure with two adjustable louvers of dimensions 1.7m x 3.7m in the east-west direction to capture wind according to the prevailing wind direction.

Figure 6. PDEC Experimental Test Facility



After wind is captured at the top, a straightener routes the wind towards a microniser spray system composed of four circuits, each circuit having a different number of nozzles, while each nozzle has a water flow rate of 7L/hr. The total number of nozzles is 20, therefore giving the facility flexibility to inject water from 7L/hr up to

140L/hr depending on external ambient conditions and indoor requirements [15].

Table 4 below shows the nozzle arrangement and injection capacity.

Table 4. Microniser Spray System

Circuit Number	Number of Micronisers	Total Flow Rate (L/hr)
1	2	14
2	4	28
3	6	42
4	8	56

Sensors were placed at five different locations at the outlet to measure temperature and relative humidity. T_M and RH_M in Table 5 represent the average measured Temperatures and Relative Humidity respectively, while T_P and RH_P represent the respective predicted temperatures and relative humidity using the CFD model. Seven cases were considered with each case having a different external ambient temperature, relative humidity and wind speed.

Table 5. Comparison between Measured and Predicted Data

Case Nb	T_M (°C)	T_P (°C)	% Error	RH_M (%)	RH_P (%)	%Error
1	27.00	28.60	5.93	75.9	74.56	1.76
2	26.00	26.16	0.62	79.4	77.07	2.93
3	26.56	27.26	2.64	76.2	72.48	4.88
4	26.90	25.65	4.65	77.4	76.04	1.75
5	25.90	25.69	0.81	72.7	71.31	1.91
6	28.78	28.24	1.88	59.9	56.72	5.30
7	28.26	27.74	1.84	62.5	62.2	0.48

Results of the CFD model and experimental data are in good agreement with maximum errors of 5.93% and 5.30% in predicting temperature and relative humidity, respectively.

CHAPTER 7

RESULTS AND PARAMETRIC ANALYSIS

Computational analysis was conducted in order to investigate the performance of an Energy Tower using CFD. Simulations were conducted using ANSYS FLUENT software version 14.5 on a 16 core PC. In this section a detailed simulation roadmap is presented to study the impact of varying:

- Water Mass Flow Rate (kg/s)
- Ambient Temperature (K)
- Outdoor Relative Humidity (%)
- Droplet Diameter (μm)
- Tower Dimensions for Height to Width Ratio of 2.5
- Tower Height to Width Ratio

For each of the above cases, the performance of the Energy Tower is investigated by studying:

- Exit Density (kg/m^3)
- Exit Temperature (K)
- Exit Velocity (m/s)
- Exit Relative Humidity (%)
- Q, which is the ratio of produced flow rate at the exit of the tower to initial flow rate.

For each of the test series sections below, three major cases are investigated, with the following parameters:

Table 6. Test Cases Designation and Parameters

	Base Case- “BC”	25°C Ambient Temperature- “T25”	50% Relative Humidity- “RH50”
Height/Diameter Ratio	2.5	2.5	2.5
Ambient Temperature (K)	309.11	298.15	309.11
External Relative Humidity (%)	13	13	50
Mixture Density (kg/m ³)	1.138	1.182	1.129
Humidity Ratio (kg/kg)	0.004755254	0.00253028	0.018696265
Droplet Temperature (K)	290	290	290
Droplet Diameter (μm)	50	50	50

7.1. Test Series I- 20m Tower

According to a height to diameter ratio of 2.5, this section investigates a 20m x 8m tower.

7.1.1. Base Case

7.1.1.1. Impact of Water Mass Flow Rate

Computational analysis was performed to study the impact of water mass flow rate on the performance of the tower. Outdoor air temperature and relative humidity are fixed at 309.11K and 13% respectively. A droplet temperature of 50μm was assumed. The water mass flow rate was increased starting from 0.31 kg/s until saturation conditions are achieved.

Figures 7 to 10 show the impact of mass flow rate on the exit average density, temperature, velocity, and relative humidity. As the injection rate increases, the mixture density increases, temperature decreases, velocity increases and relative humidity increases, consistent with the dynamics of evaporation. Near saturation conditions, the rate of change decreases as the air conditions since less room for evaporation is available. A maximum temperature decrease observed is 290.5K, which is a drop of 18.61°C and a velocity of 4.5m/s can be achieved.

Figure 7. Tower 20x8- Base Case- Exit Density vs. Injection Rate

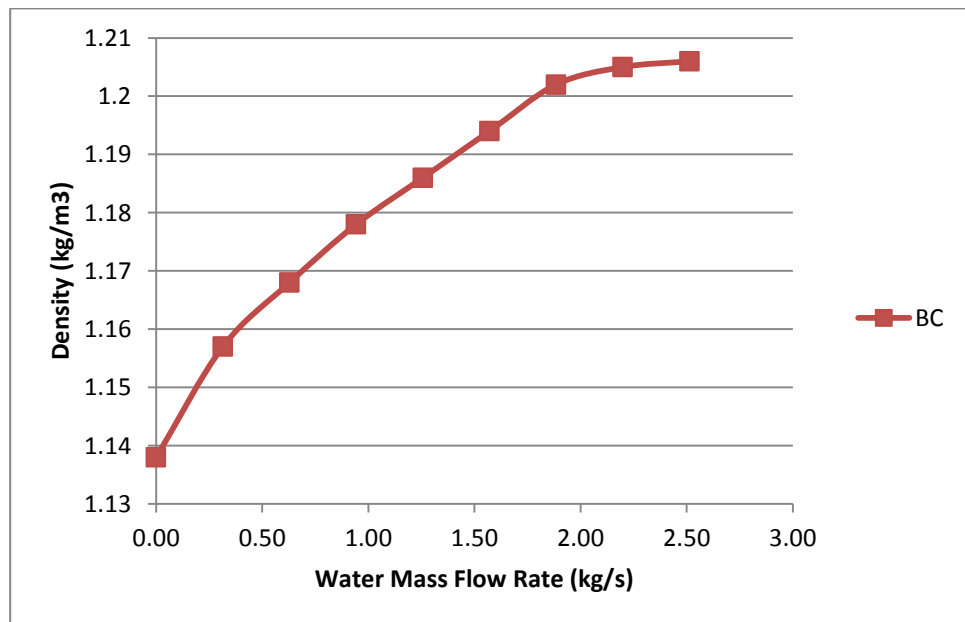


Figure 8. Tower 20x8- Base Case- Exit Velocity vs. Injection Rate

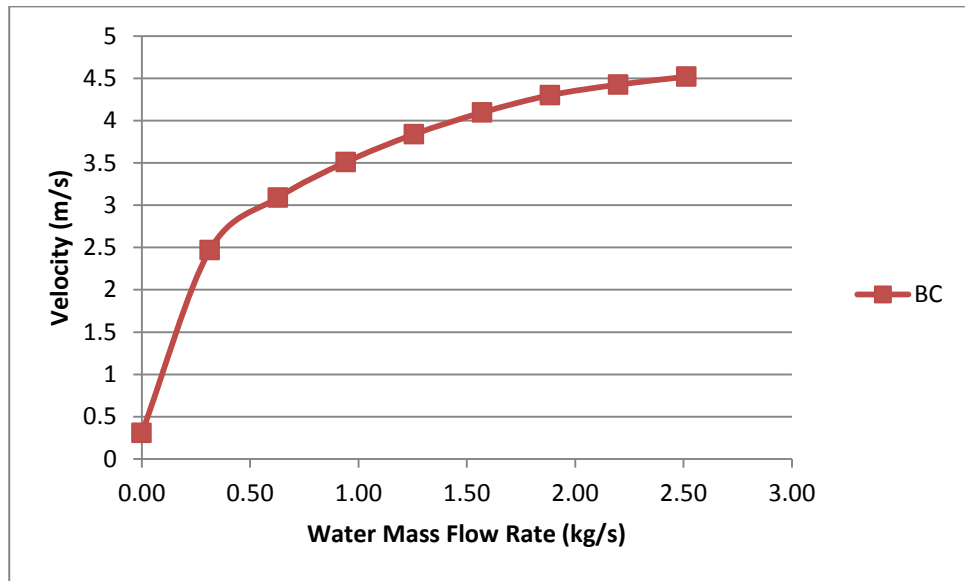


Figure 9. Tower 20x8- Base Case- Exit Temperature vs. Injection Rate

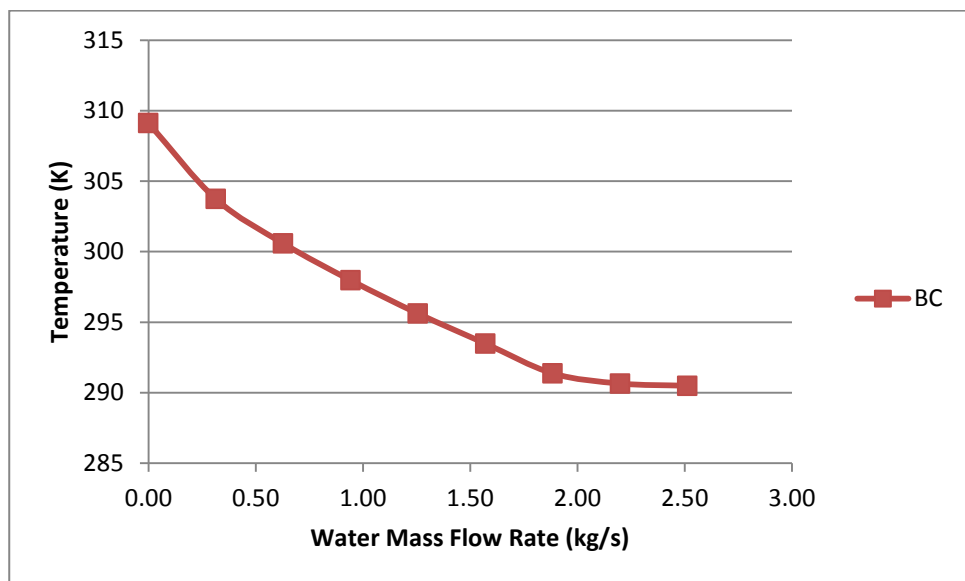


Figure 10. Tower 20x8- Base Case- Exit Relative Humidity vs. Injection Rate

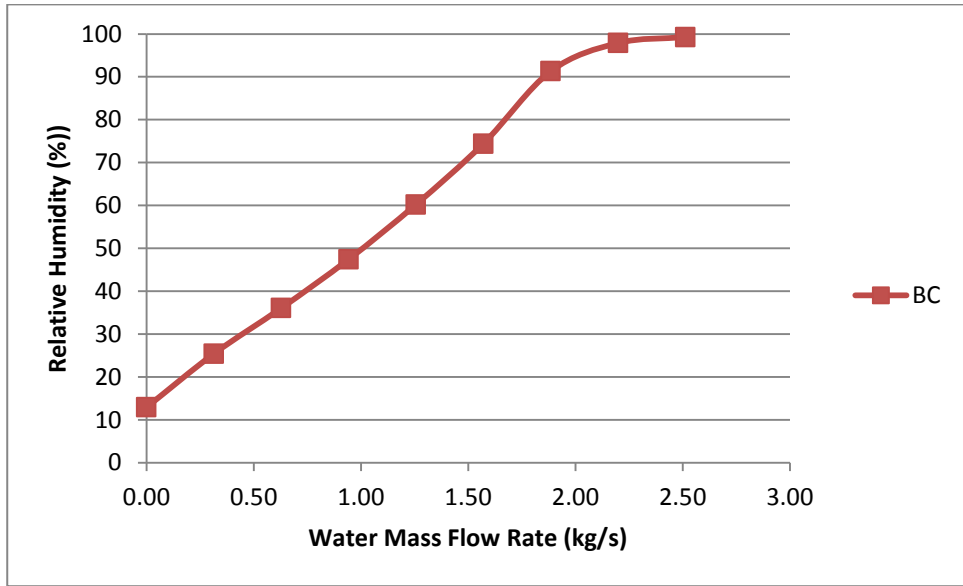
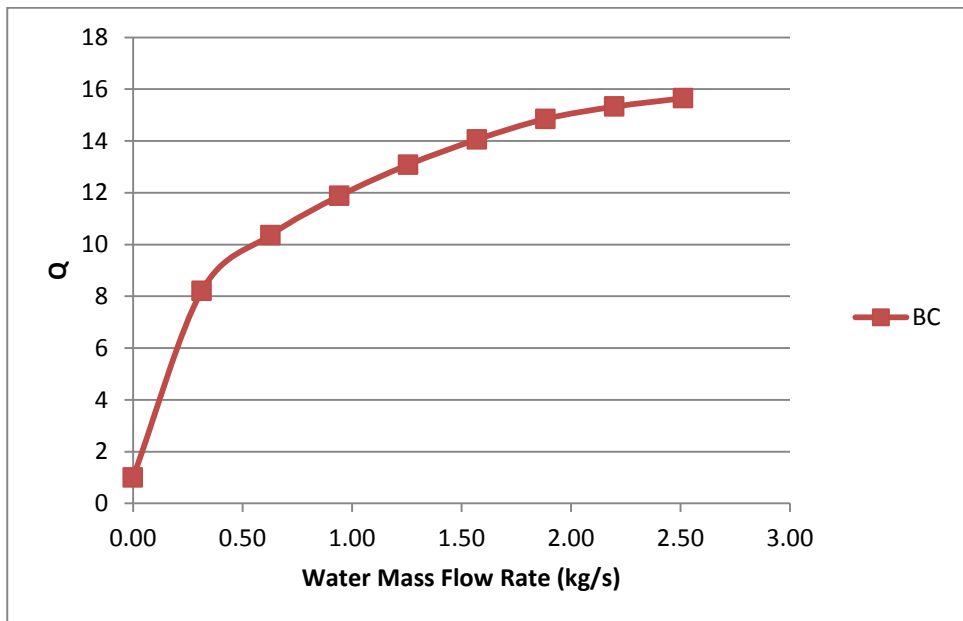


Figure 11 shows the variation Q (ratio of mass flow rate produced to initial mass flow rate prior to injection) as the injection rate increases. Injecting only 0.31kg/s of water produces 8.2 times the flow. A ratio of 15.6 is witnessed at saturation (injection of 2.51 kg/s of water).

Figure 11. Tower 20x8- Base Case- Q vs. Injection Rate



Air conditions are compared to verify how the increase of mass flow rate impacts of the evolution of the flow field within the effective area of the tower and along a line which passes exactly through the middle of the tower.

Figures 12 to 14 show the contours of density for three representative water mass flow rates (0.31kg/s, 1.26 kg/s and 2.51 kg/s).

For a low injection rate, 0.31kg/s, towards the top of the tower, all water droplets have evaporated. As the injection rate increases, the flow field is capable of absorbing additional mass until saturation is achieved and the density no longer changes and reaches its maximum value.

Figure 12. Tower 20x8- BC- Contour of Density for Injection Rate 0.31kg/s

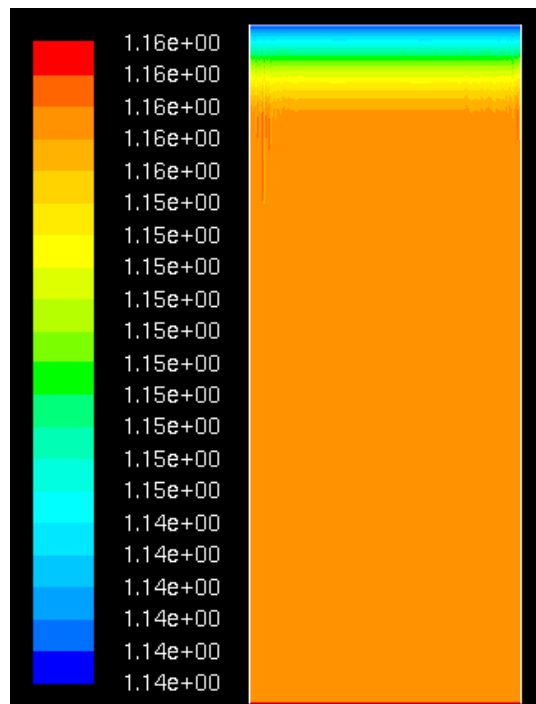


Figure 13. Tower 20x8- BC- Contour of Density for Injection Rate 1.26kg/s

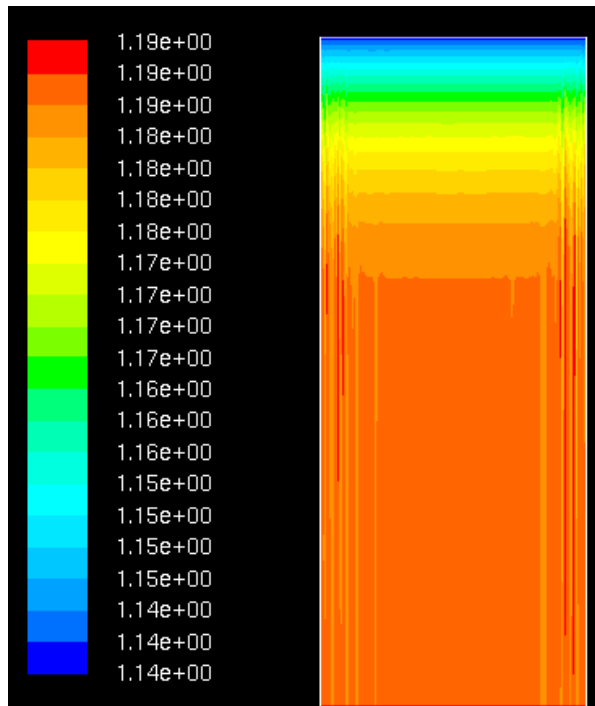
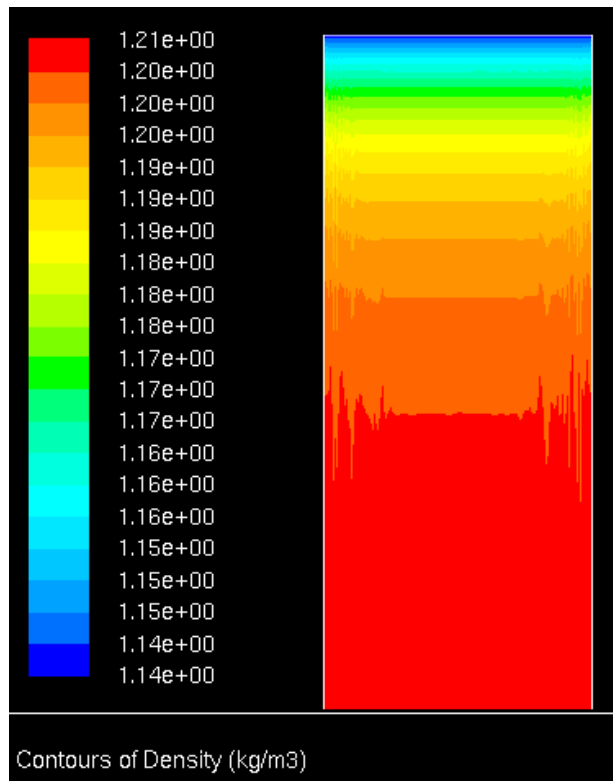


Figure 14. Tower 20x8- BC- Contour of Density for Injection Rate 2.51kg/s



Figures 15 to 17 show the contours of temperature for three representative water mass flow rates (0.31kg/s, 1.26 kg/s and 2.51 kg/s).

Figure 15. Tower 20x8- BC- Contour of Temperature for Injection Rate 0.31kg/s

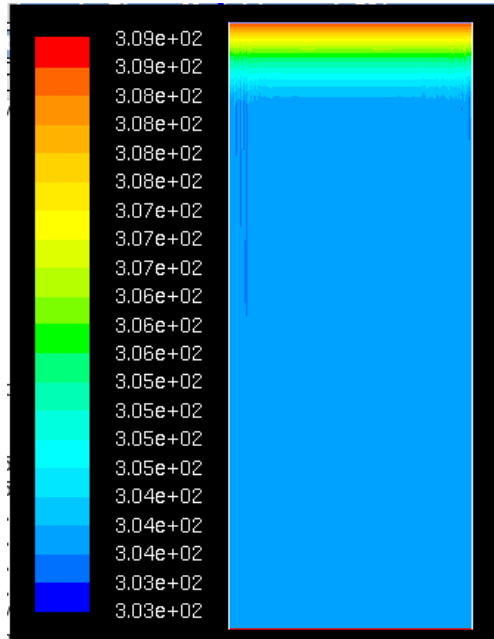


Figure 16. Tower 20x8- BC- Contour of Temperature for Injection Rate 1.26kg/s

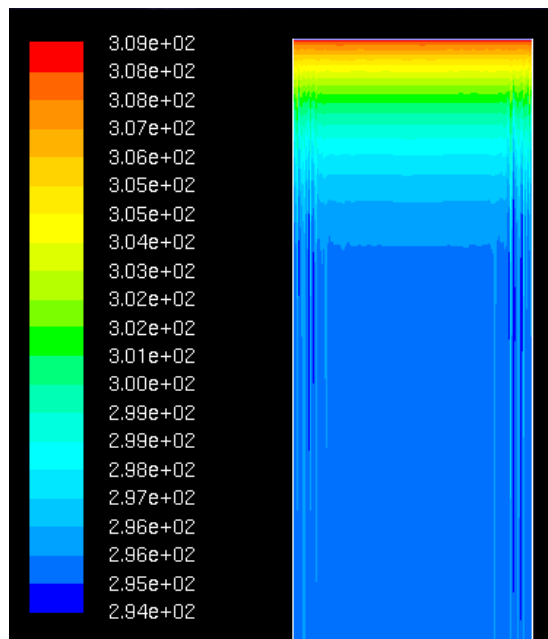
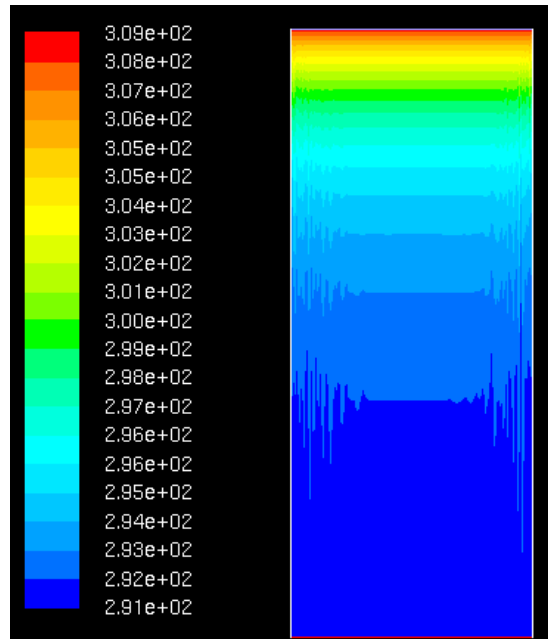


Figure 17. Tower 20x8- BC- Contour of Temperature for Injection Rate 2.51kg/s



Figures 18 to 20 show the contours of relative humidity for three representative water mass flow rates (0.31kg/s, 1.26 kg/s and 2.51 kg/s).

Figure 18. Tower 20x8- BC- Contour of RH for Injection Rate 0.31kg/s

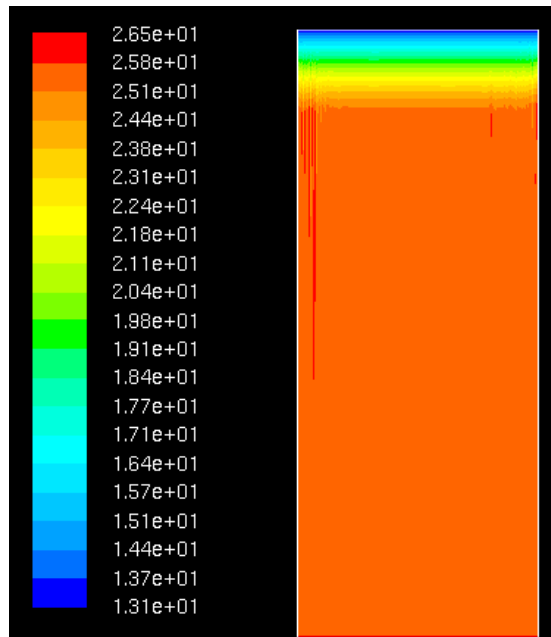


Figure 19. Tower 20x8- BC- Contour of RH for Injection Rate 1.26kg/s

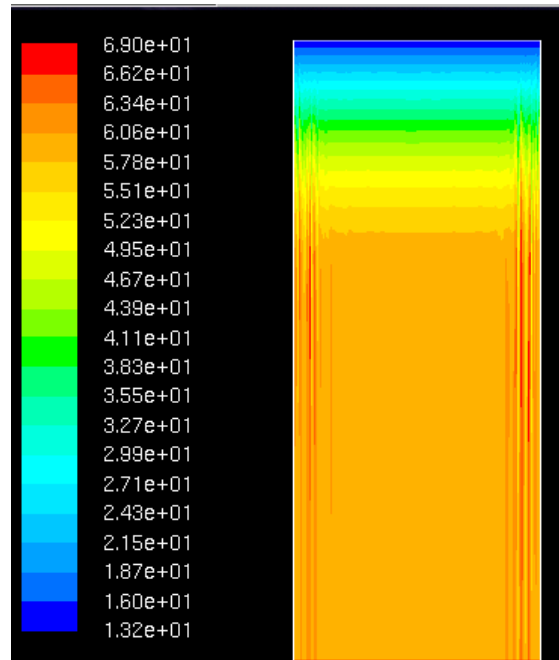
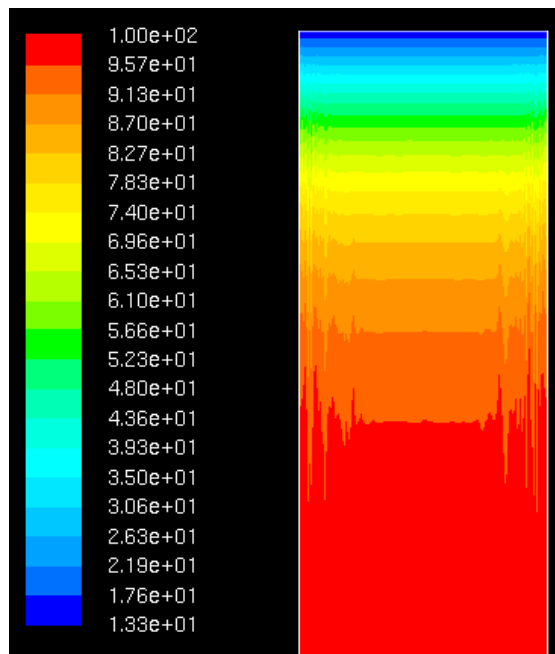


Figure 20. Tower 20x8- BC- Contour of RH for Injection Rate 2.51kg/s



Figures 21 to 23 show the behavior of humid air, temperature and relative humidity respectively along a line which passes exactly through the middle of the tower. For a low injection rate, all droplets evaporate at the top of the tower and the properties become constant until the flow exits the tower. As the injection rate increases, the evaporation process becomes more gradual. For a high enough injection rate which renders exit conditions above 90% relative humidity, injecting more water has a minor impact on exit conditions.

Figure 21. Tower 20x8-BC- Evolution of Density from Inlet to Outlet vs. Injection Rate

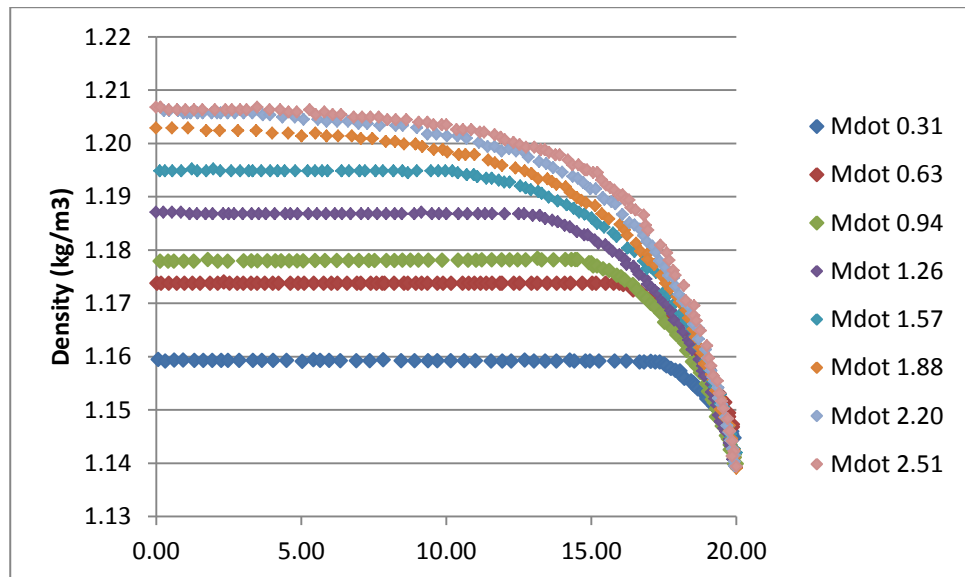


Figure 22. Tower 20x8-BC- Evolution of Temperature from Inlet to Outlet vs. Injection Rate

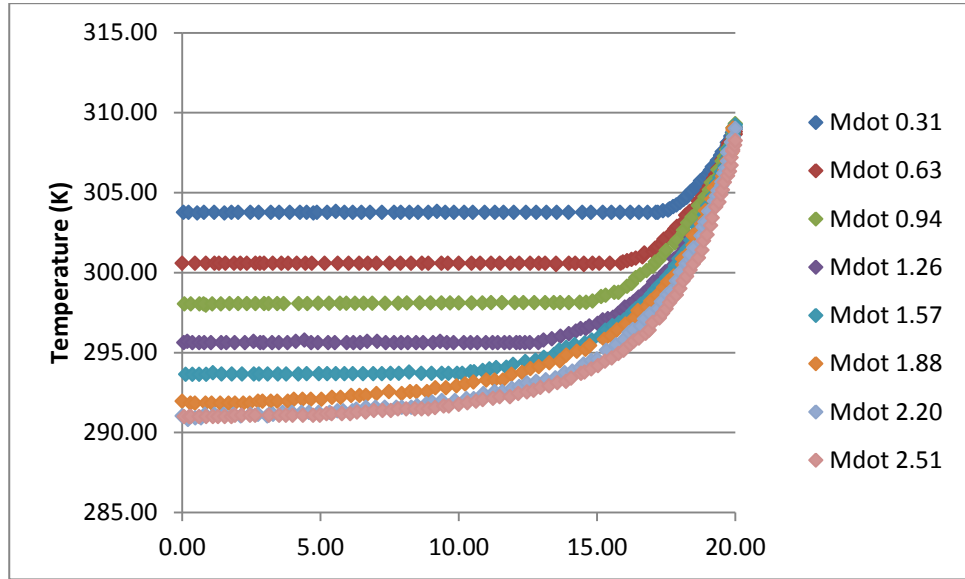
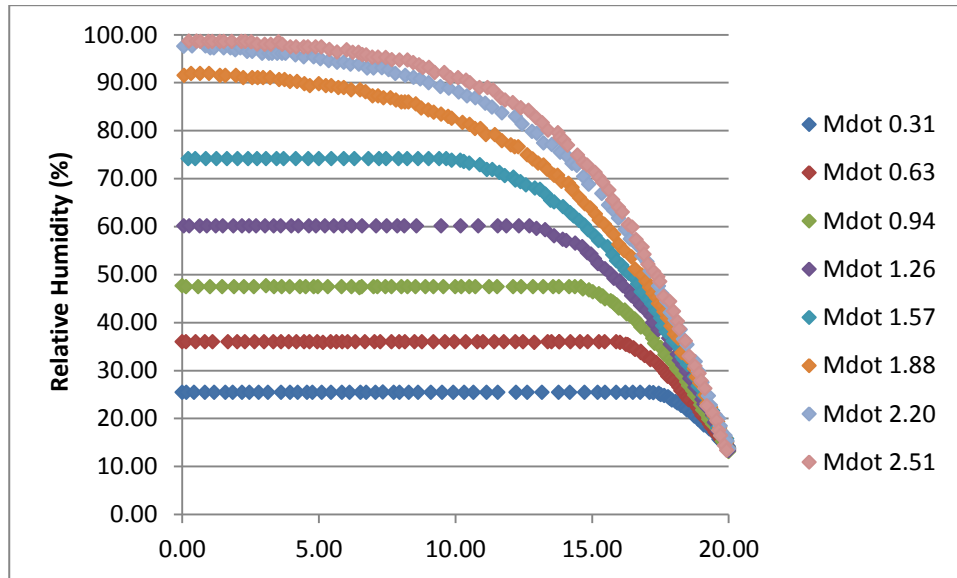


Figure 23. Tower 20x8-BC- Evolution of RH from Inlet to Outlet vs. Injection Rate



7.1.1.2. Impact of Droplet Diameter

In this section, the impact of varying droplet diameter is studied. Carlson [1] suggested that the droplet diameter should not exceed 100 μ m. Zaslavsky [2] argued that decreasing droplet diameter below 100 μ m would require a significant energy

investment and in fact should be in the range between $150\mu\text{m}$ to greater than $500\mu\text{m}$. Since the evaporation process is gradual rather than instantaneous, the excess weight of the droplets that have not yet evaporated is claimed to enhance the downdraft.

In this study, the droplet size is varied between $50\mu\text{m}$ and $300\mu\text{m}$ in steps of 50. Figures 24 to 26 show the evolution of humid air, temperature, and relative humidity respectively along a line which passes exactly through the middle of the tower under variable droplet size. The mass flow rate of water is kept constant at 0.63kg/s for all cases.

As the droplet diameter increases, the evaporation processes is decelerated. The difference in temperature drop from ambient temperature between the lowest droplet diameter and the highest is 8.5°C and 5.3°C respectively, while the difference in relative humidity increase between the lowest droplet diameter and the highest is 23.07% and 12.18% respectively. However, a bigger temperature drop was witnessed for a diameter of $100\mu\text{m}$ rather than $50\mu\text{m}$ indicating highest wet bulb depression capability over the height of the tower, for the later.

Figure 24. Tower 20x8-BC- Evolution of Density from Inlet to Outlet vs. Droplet Diameter

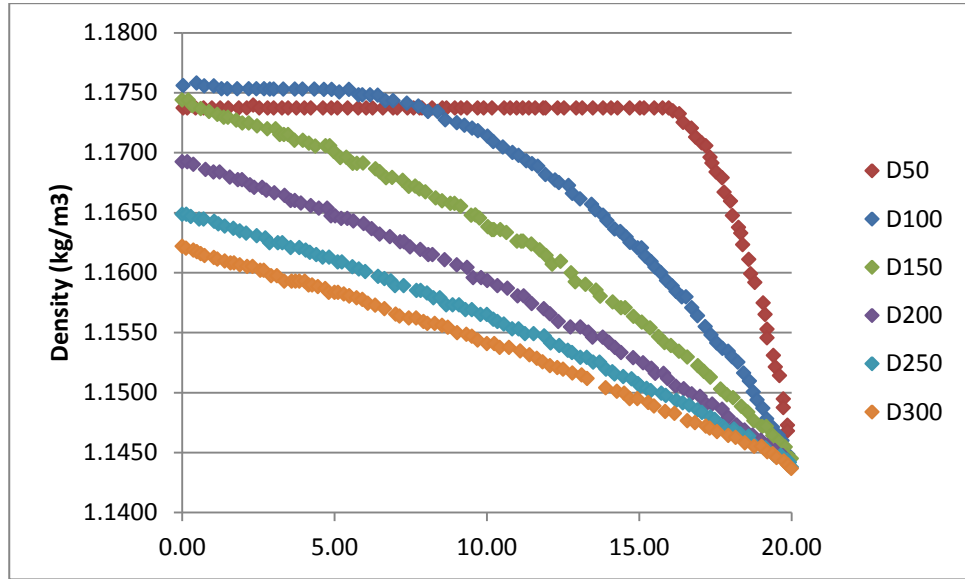


Figure 25. Tower 20x8-BC- Evolution of Temperature from Inlet to Outlet vs. Droplet Diameter

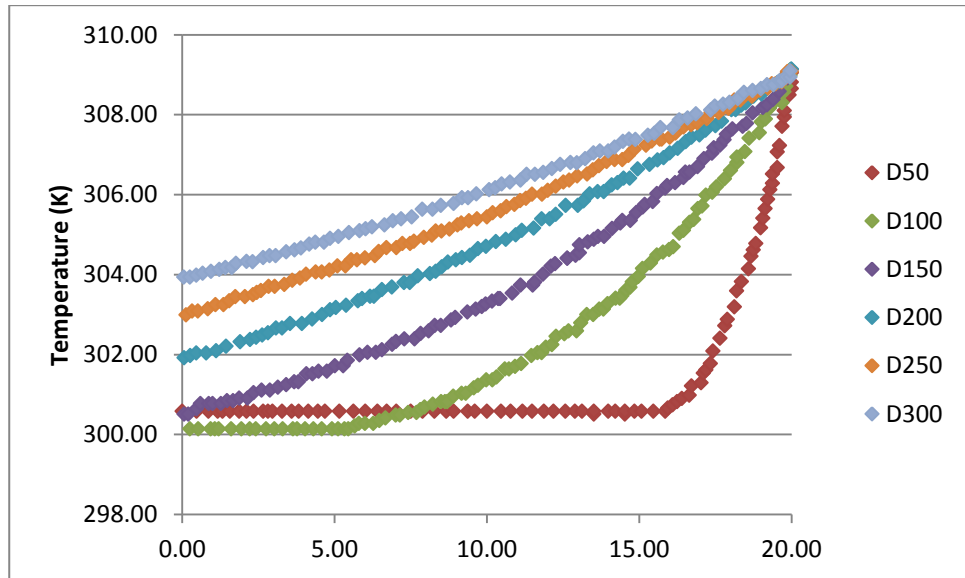
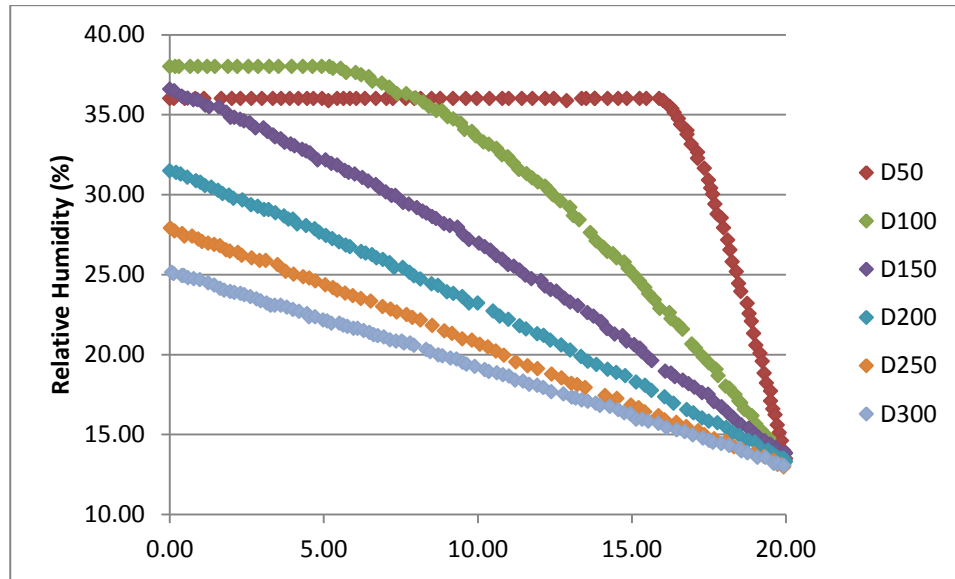


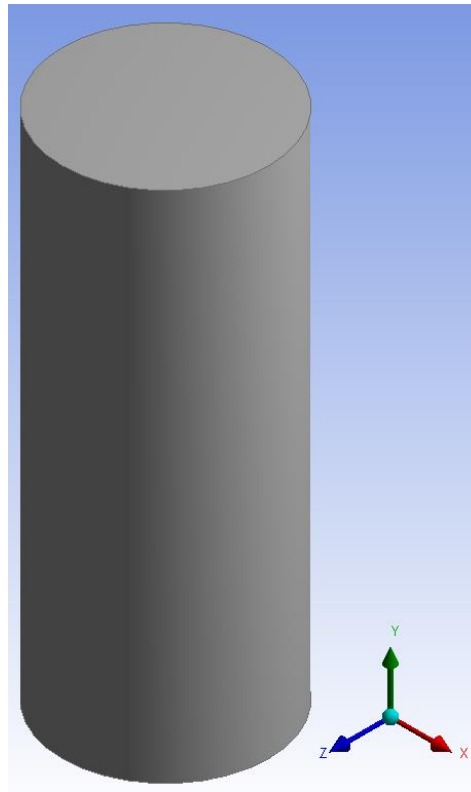
Figure 26. Tower 20x8-BC- Evolution of RH from Inlet to Outlet vs. Droplet Diameter



7.1.1.3. 3D Simulation

In this section, results of the 2D simulation are validated against a 3D model in order to verify that results in 2D remain effective in 3D. A 20 meter cylindrical tower with diameter of 8 meters (Figure 27) is studied. The exact model that was implemented in 2D is reproduced for the 3D case.

Figure 27. 3D Tower (20m)



Figures 28 to 31 show the average exit conditions of the flow field between 2D and 3D simulations, after mapping injection rates used in 2D simulations.

Figure 28. Average Exit Density (2D vs. 3D)

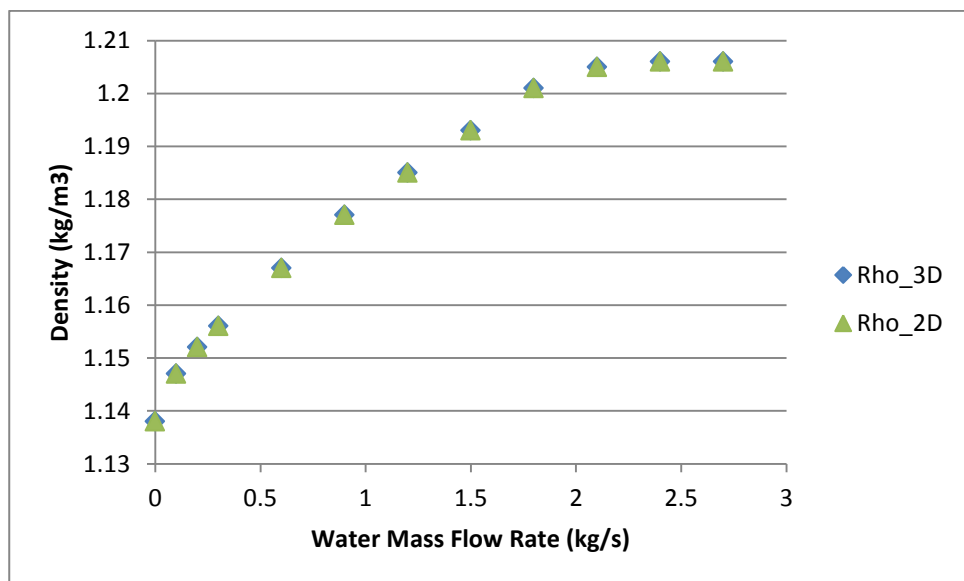


Figure 29. Average Exit Velocity (2D vs. 3D)

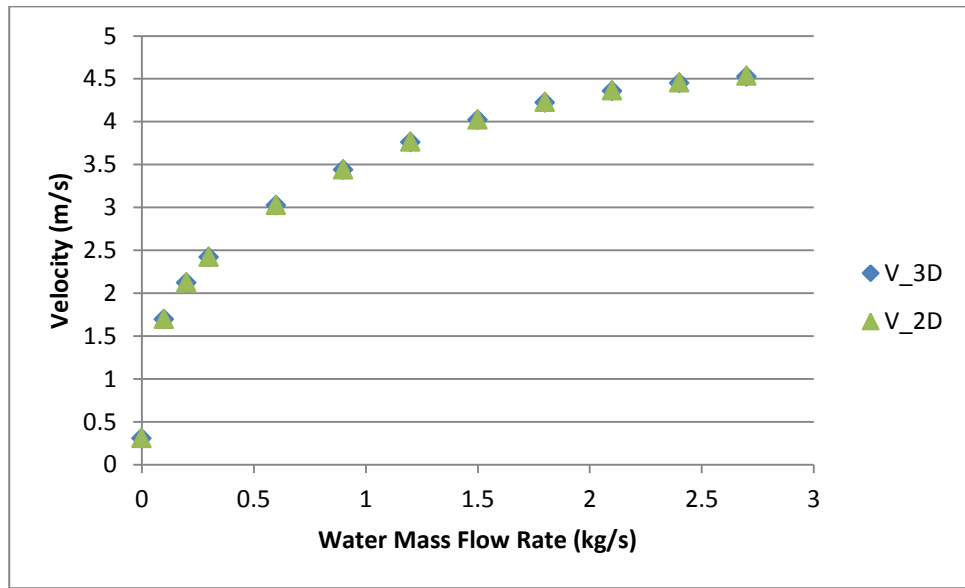


Figure 30. Average Exit Temperature (2D vs. 3D)

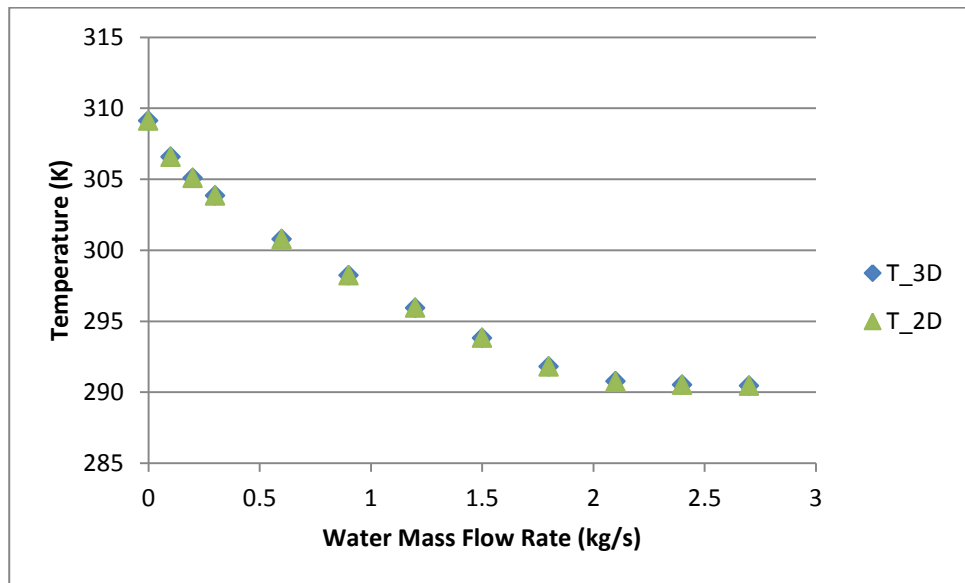
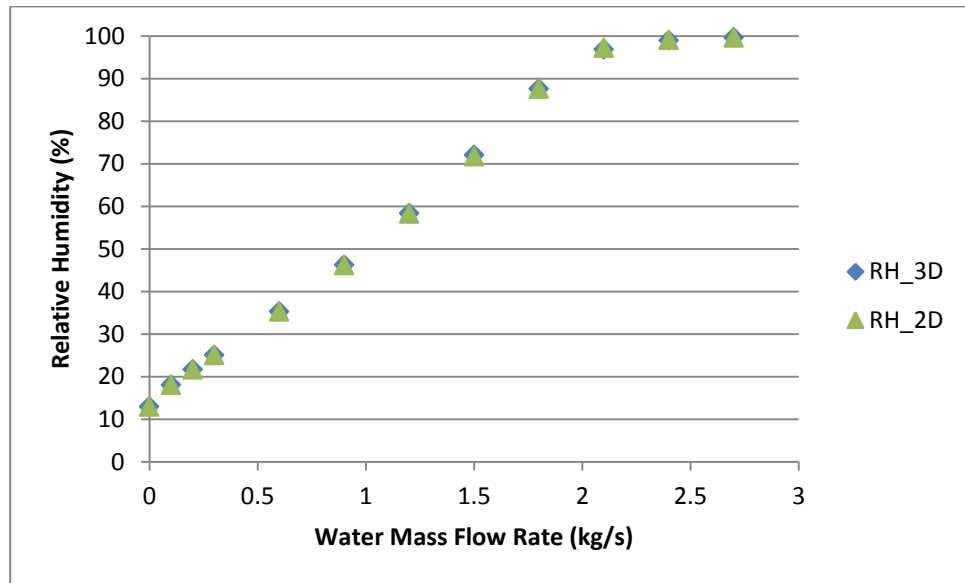


Figure 31. Average Exit RH (2D vs. 3D)



Results show overlapping trends between 2D and 3D, and therefore results remain valid in 3D simulations.

7.1.2. Impact of Varying Ambient Temperature and Outdoor Relative Humidity

In this section, the effect of varying ambient temperature and outdoor relative humidity on the flow field is studied.

Outdoor temperatures of 20°C, 25°C, and 30°C are considered, designated as T20, T25 and T30 respectively. Similarly, outdoor relative humidity of 25%, 50%, and 75% is considered, designated as RH25, RH50, and RH75 respectively.

Figures 32 to 38 show the impact of injection rate on exit conditions of the tower for all cases. The energy tower performs best under the base case, which is the hottest and driest condition, whereby the highest velocity is achieved of 4.5 m/s and

the highest amount of mass is produced. The lowest velocity of 3.1m/s is achieved when the relative humidity is highest (75%).

The highest temperature drop is achieved for the hottest and driest outdoor condition (Base Case) with a temperature drop of 18.62°C. The lowest drop is witnessed in the most humid condition (RH75), with a drop of 4.26°C.

Table 7. Tower 20x8- Temperature Drop

	BC	T20	T25	T30	RH25	RH50	RH75
Ambient Temperature (K)	309.11	293.15	298.15	303.15	309.11	309.11	309.11
Exit Temperature (K)	290.49	281.25	284.15	286.93	293.79	300.01	304.84
Temperature Drop	18.62	11.89	13.99	16.21	15.31	9.10	4.26

Figure 32. Tower 20x8- Q vs. Injection Rate

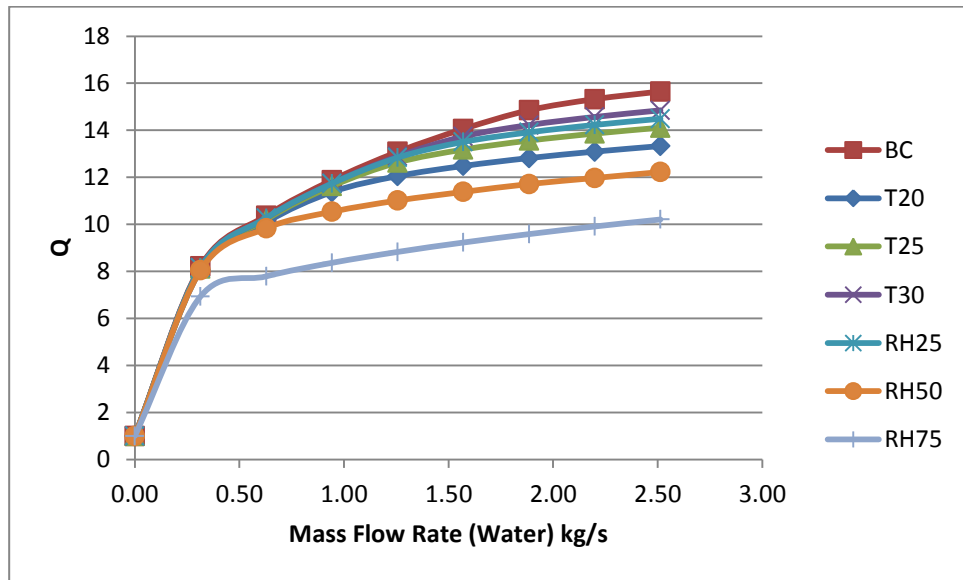


Figure 33. Tower 20x8- Density vs. Injection Rate

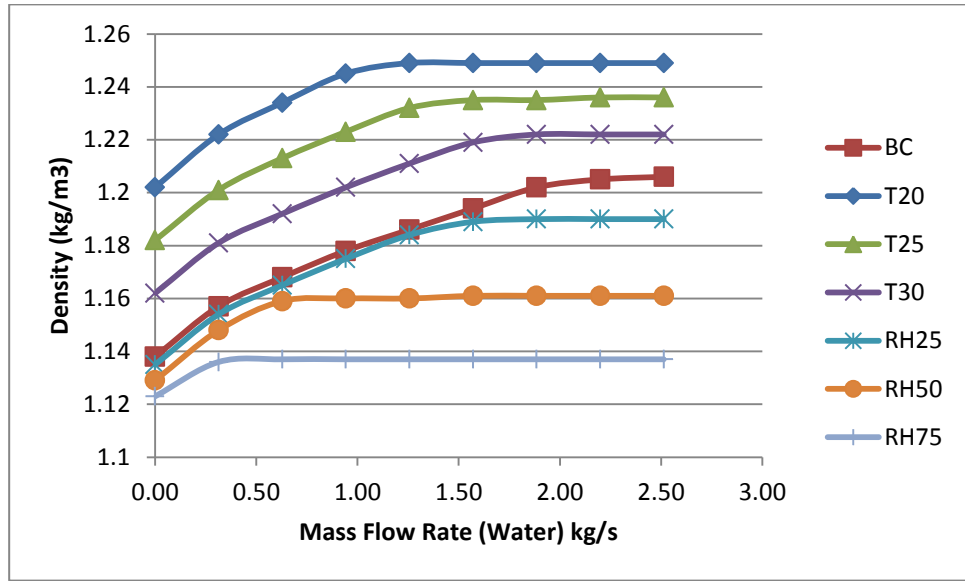


Figure 34. Tower 20x8- Velocity vs. Injection Rate

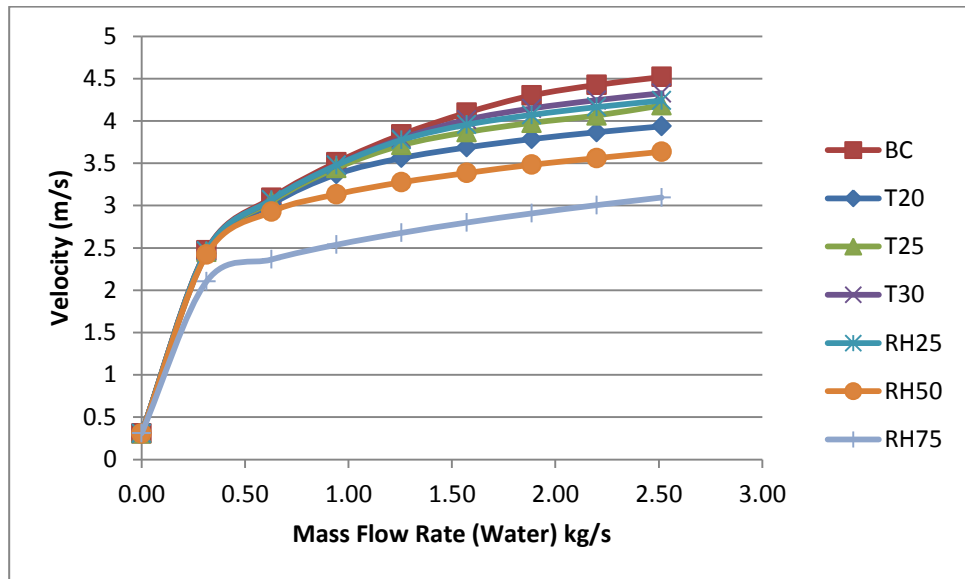


Figure 35. Tower 20x8- Temperature vs. Injection Rate

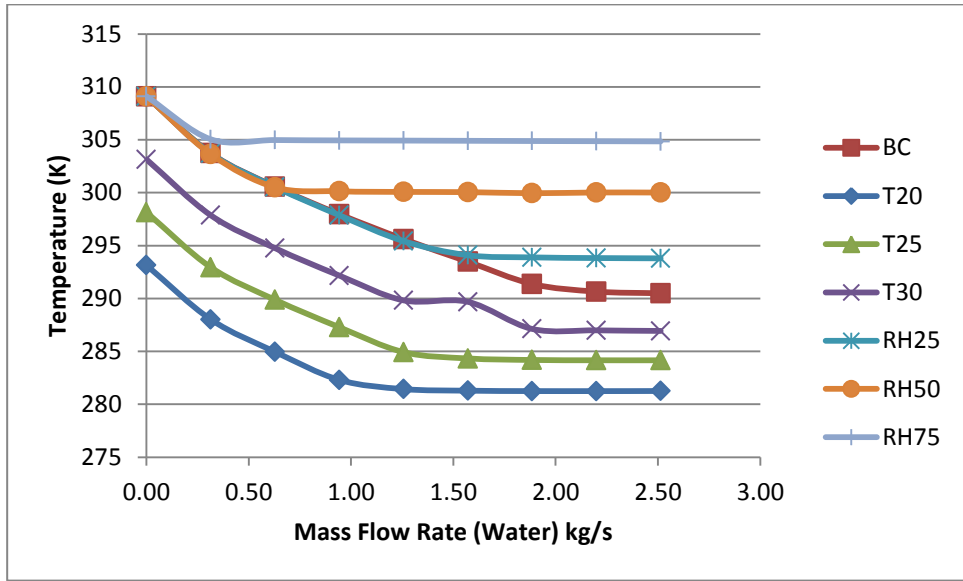


Figure 36. Tower 20x8- Relative Humidity vs. Injection Rate

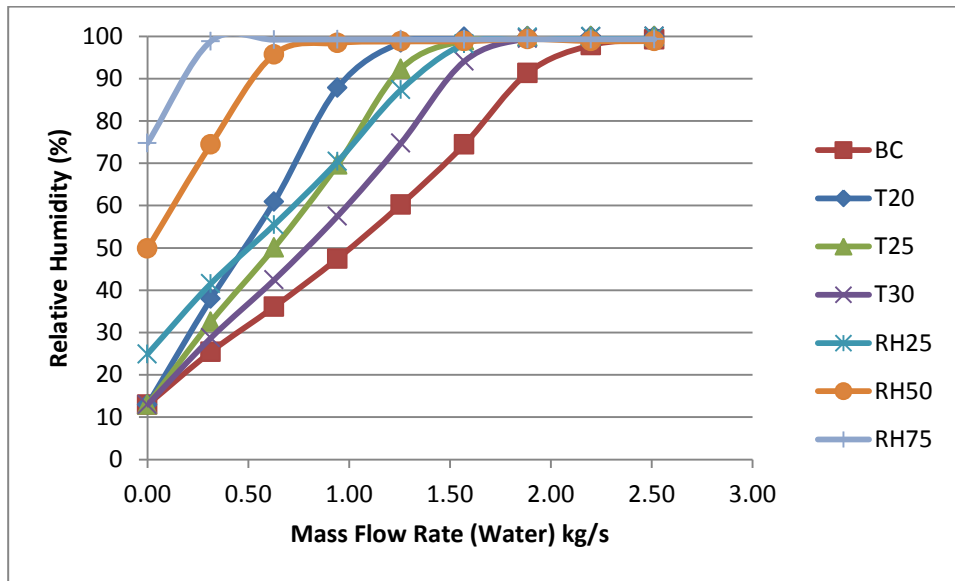


Figure 37. Tower 20x8- Exit Velocity vs. Temperature

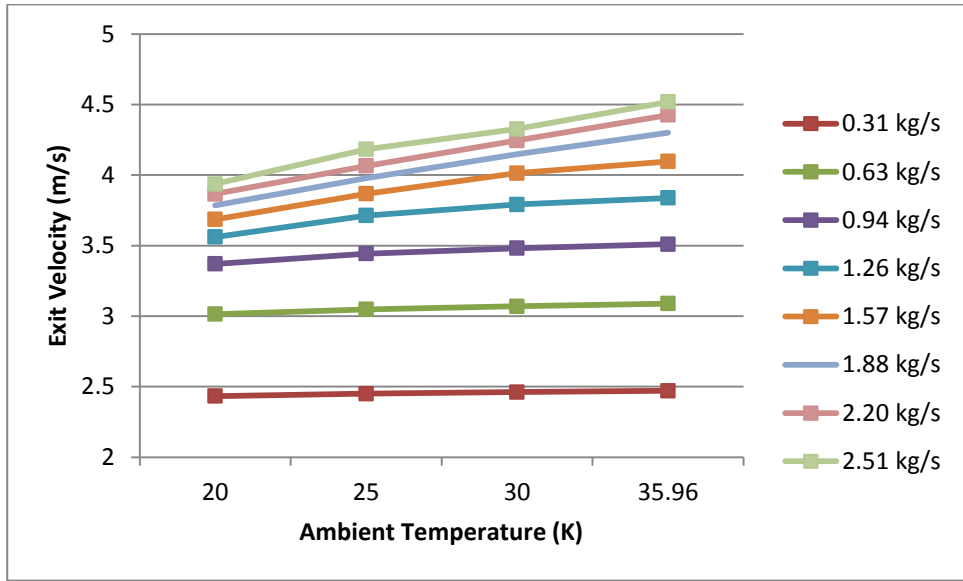
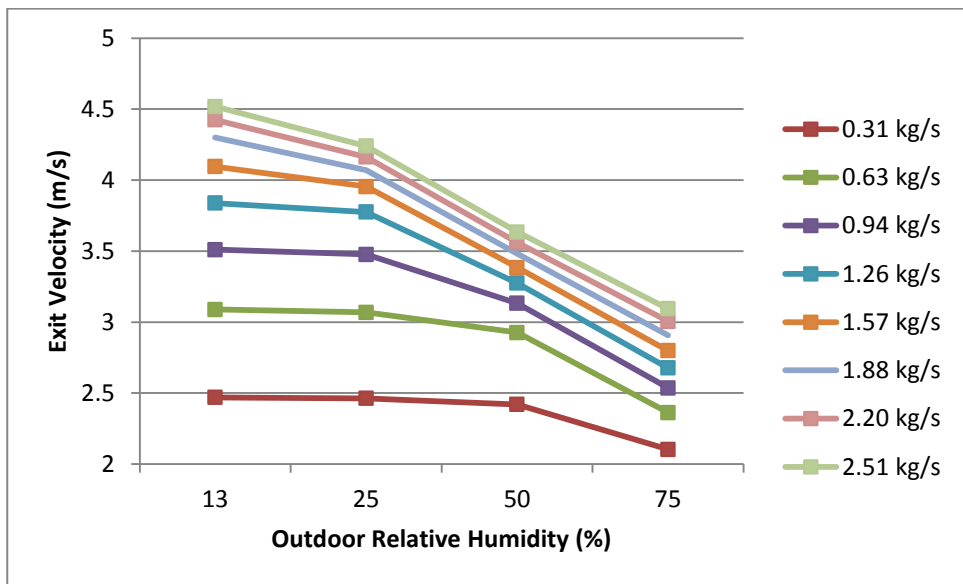


Figure 38. Tower 20x8- Exit Velocity vs. Outdoor Relative Humidity



7.2. Test Series II- 100m Tower

In this section, a 100m x40m Tower is investigated. Similar to the Analysis conducted in 7.1, the impact of Injection Rate and Droplet Diameter is studied over three representative cases highlighted in Table 4.

7.2.1. Impact of Water Mass Flow Rate

The injection rate is increased from 3.14 kg/s until saturation is achieved.

Figures 39 to 43 show the impact of increasing water injection rate on exit conditions.

Over a 100 meter tower, a velocity of 10.6m/s is achievable over a hot dry condition (Base Case) followed by 9.6 m/s for a cold dry condition (T25) and 8.3 m/s for a hot humid condition (RH50). The same exit conditions of temperature and density are observed as the case of the 20x8 tower, because injection rate requirements increase due to inlet area increase, but the external conditions are the same therefore exit density and temperature should not change. Yet, the greater the inlet area, the more we can produce wind and make use of our environment and this is evident as the ratio of quantity of mass that can be produced is 36.6 for the base case of a 100m tower at saturation versus 15.56 for the base case of a 20m tower at saturation. A similar trend for relative humidity is observed over 100m tower as the 20m tower.

Figure 39. Tower 100x40- Q vs. Injection Rate

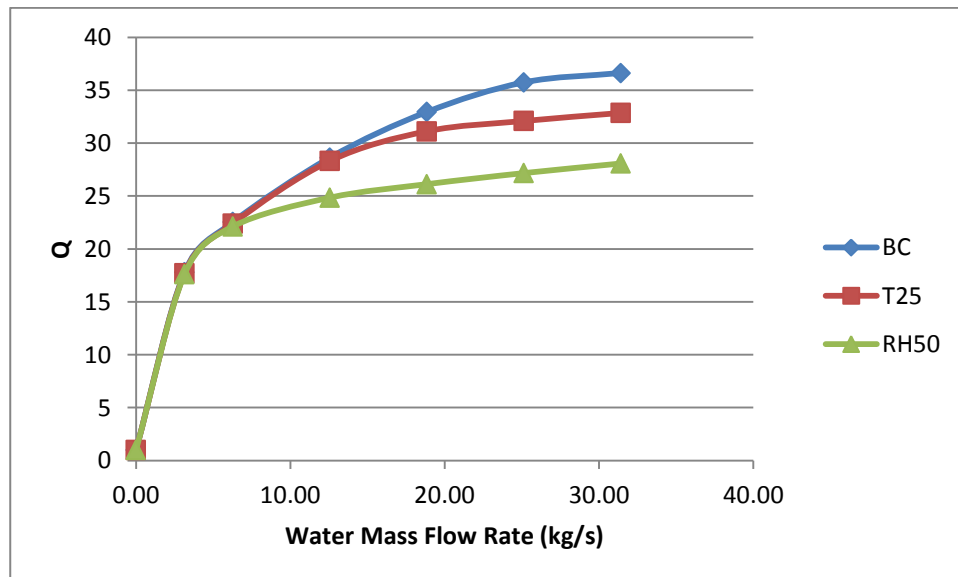


Figure 40. Tower 100x40- Density vs. Injection Rate

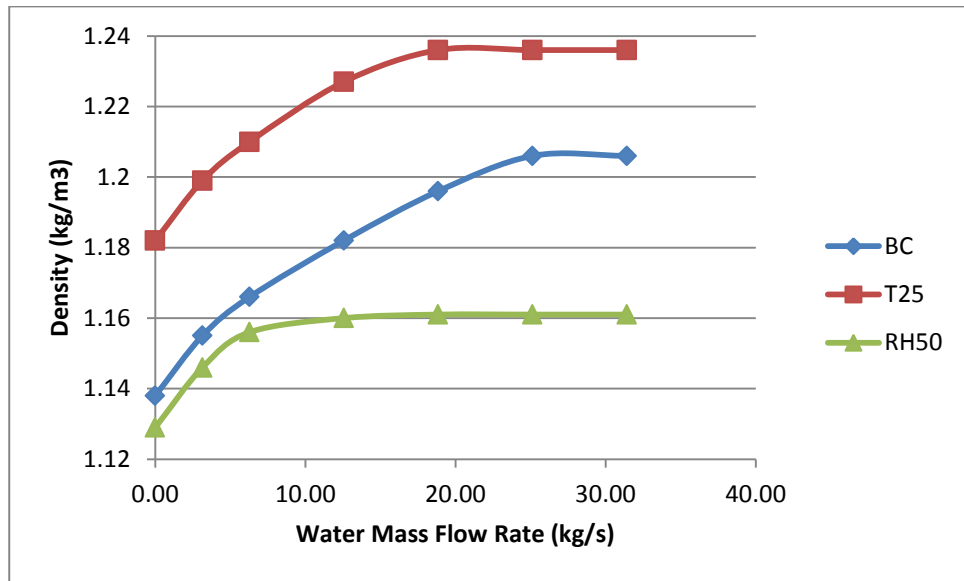


Figure 41. Tower 100x40- Velocity vs. Injection Rate

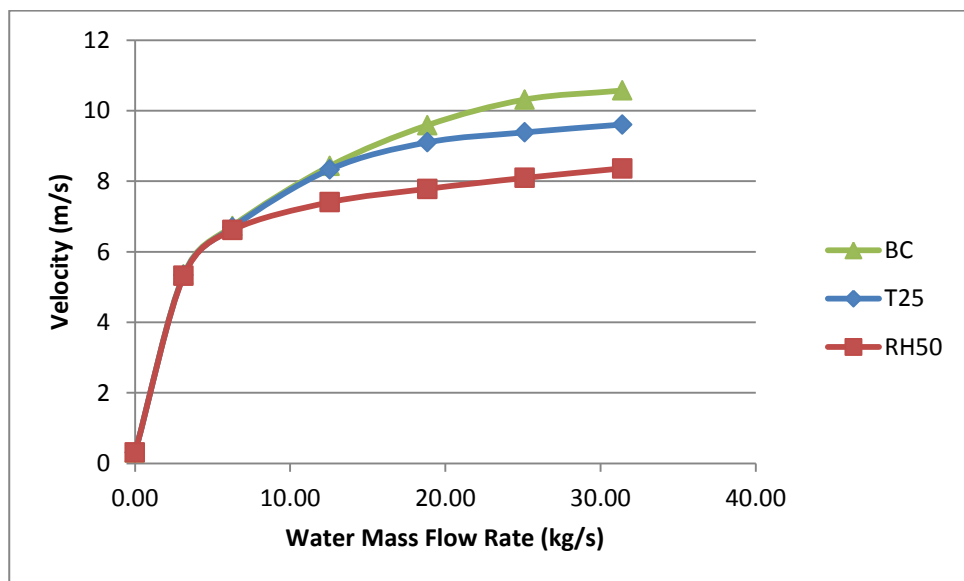


Figure 42. Tower 100x40- Temperature vs. Injection Rate

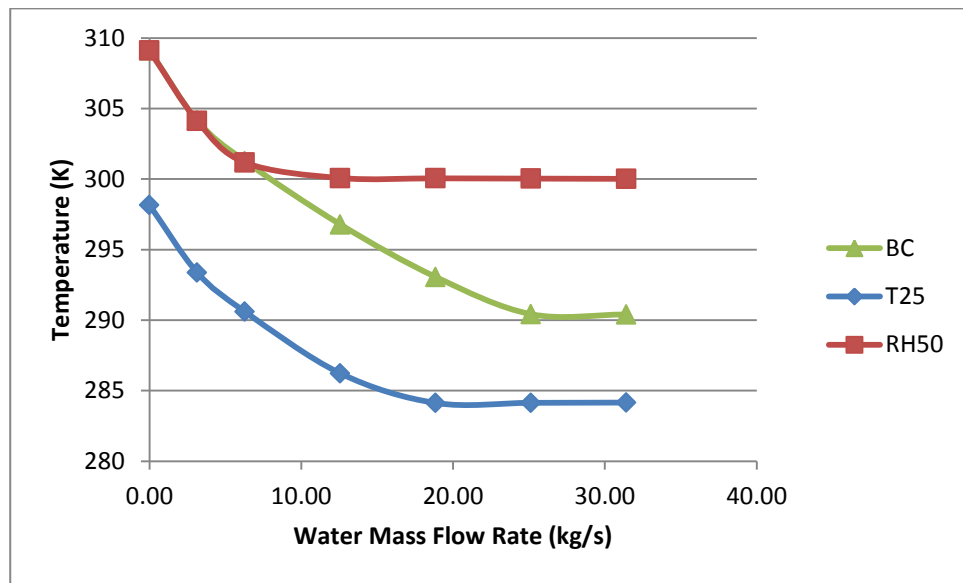
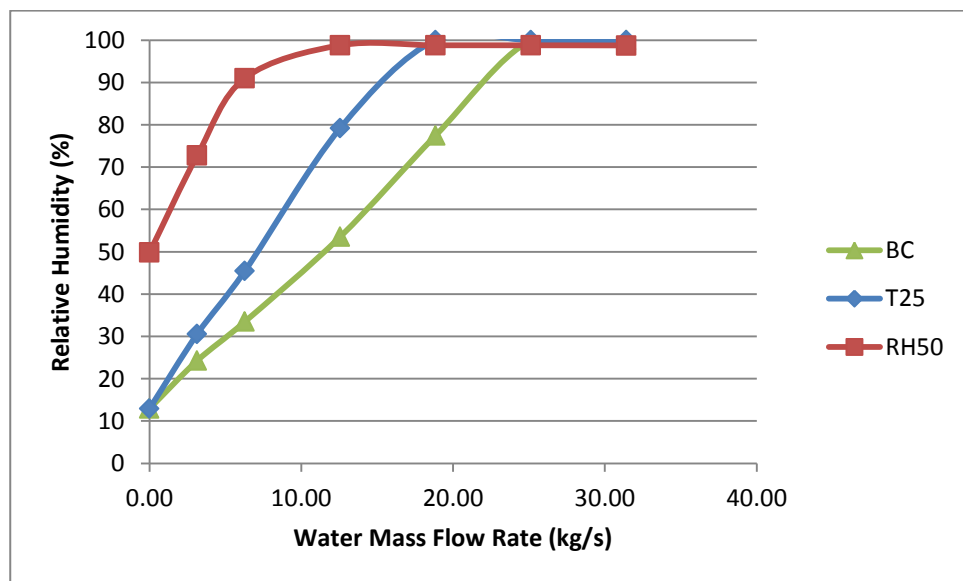


Figure 43. Tower 100x40- Relative Humidity vs. Injection Rate



7.2.2. Impact of Droplet Diameter

The Impact of Droplet Diameter on Variables is investigated in this section for a water injection rate of 6.28 kg/s.

Figures 44 to 48 show the impact of droplet diameter on the flow field. The lowest temperature witnessed for the Base Case was 300.45K for a droplet diameter of

200 μm , and for T25 a temperature low of 289.90K for a droplet diameter of 150 μm , and for RH50 a temperature low of 300.10K for a droplet diameter of 100 μm . At each temperature low value, we can see the highest density value since the cooler the humid air, the higher is its density. Trends of density and relative humidity are similar and inverse to trends of temperature.

As the droplet diameter increases, velocity decreases and therefore the quantity of mass that is produced decreases.

Figure 44. Tower 100x40- Q vs. Droplet Diameter

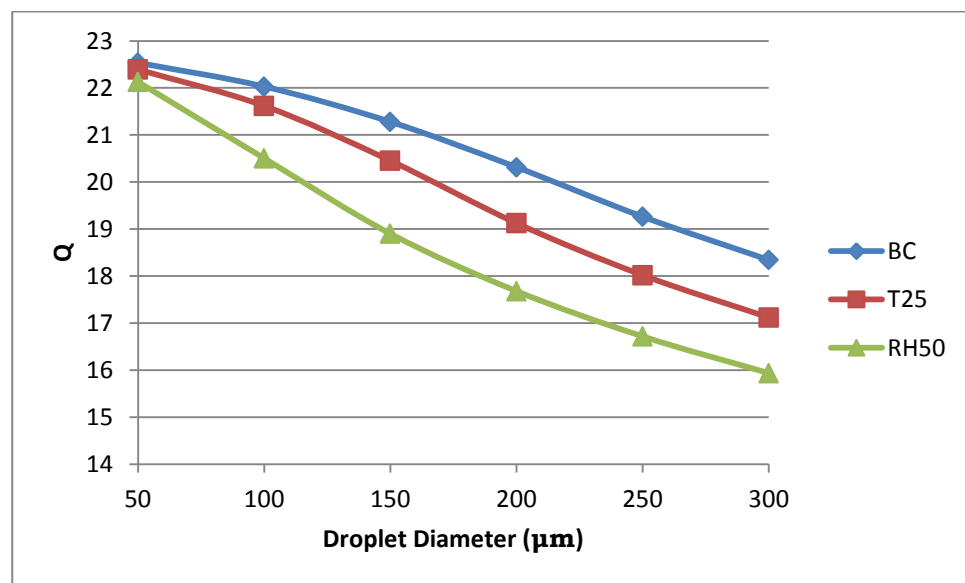


Figure 45. Tower 100x40- Density vs. Droplet Diameter

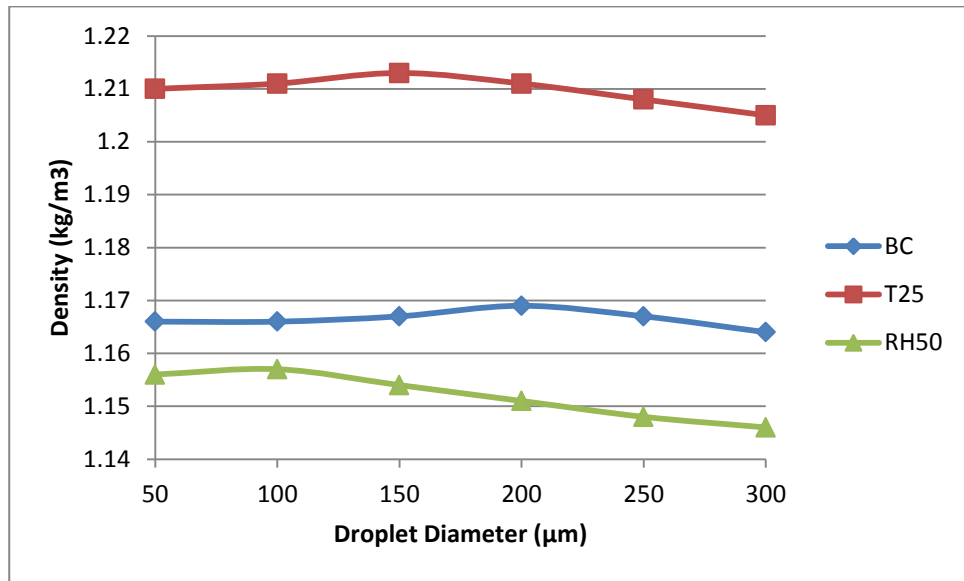


Figure 46. Tower 100x40- Velocity vs. Droplet Diameter

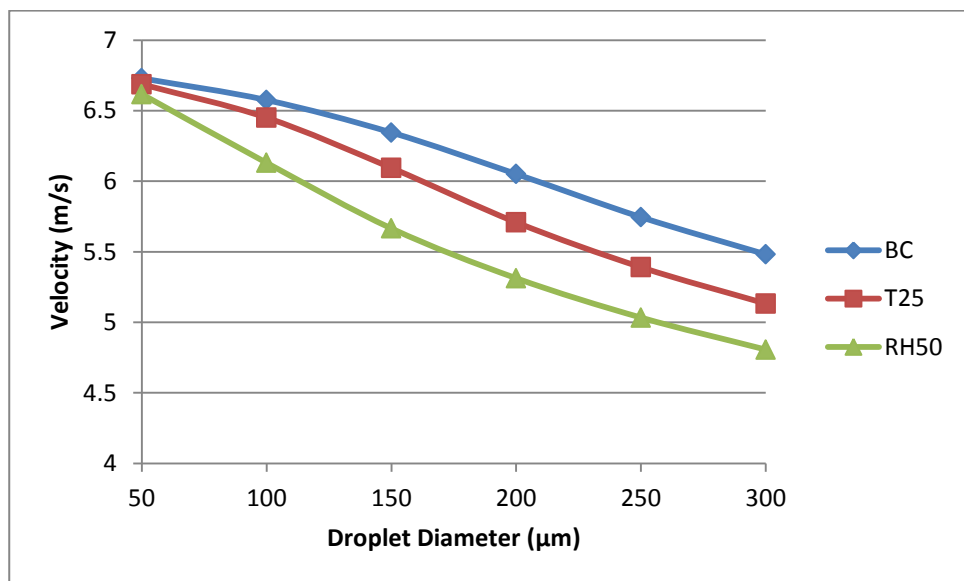


Figure 47. Tower 100x40- Temperature vs. Droplet Diameter

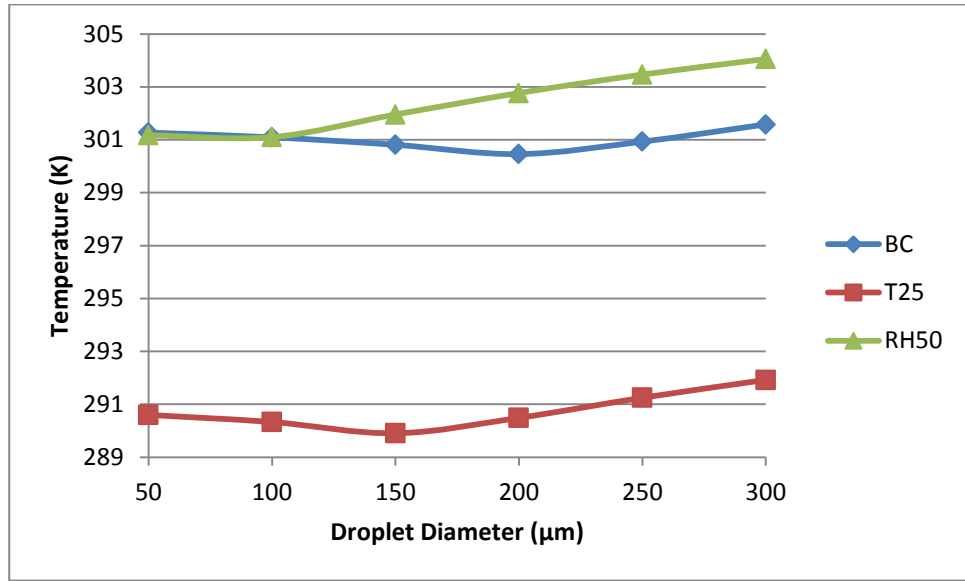
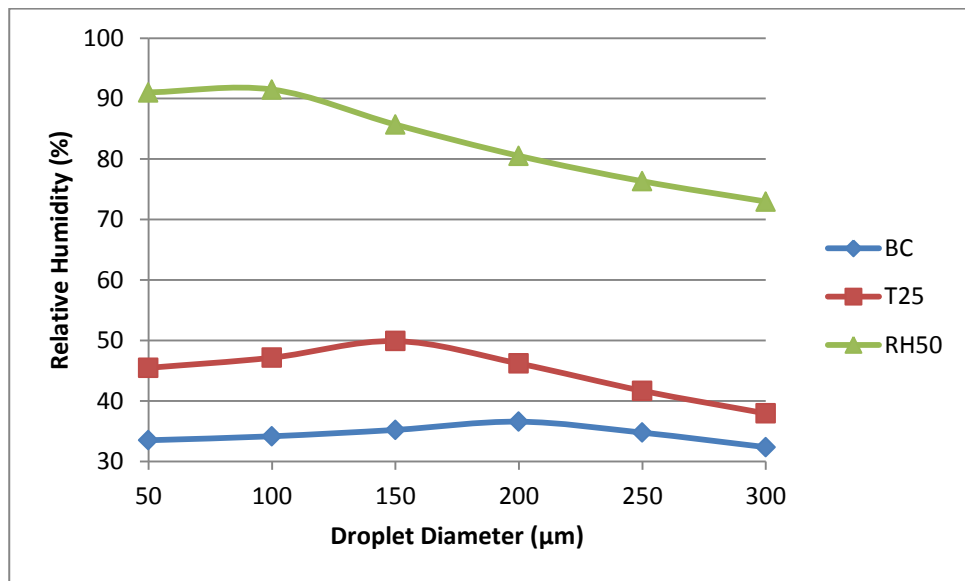


Figure 48. Tower 100x40- Relative Humidity vs. Droplet Diameter



7.3. Test Series III- 400m Tower

Simulations were conducted on a 400m tower with diameter of 160m. Under this series, the impact of changing tower diameter is investigated for height to diameter ratios of 1.5 and 2.5.

7.3.1. Impact of Water Mass Flow Rate

In this section, the water mass flow rate was increased from 25.13 kg/s up until saturation conditions are achieved.

Similar to the simulations conducted on a 20m and 100m tower, at saturation, the exit conditions of temperature and density are the same, as is the trend. For a 400m tower, an exit velocity of 21 m/s is achieved for the base case, 19 m/s for an ambient temperature of 25 °C, and 16.3m/s when the outdoor relative humidity is 50%. This translates to producing 72.4, 64.9, and 54.4 times mass when injecting 200 kg/s of water, for each of the three cases respectively.

Figure 49. Tower 400x160- Q vs. Injection Rate

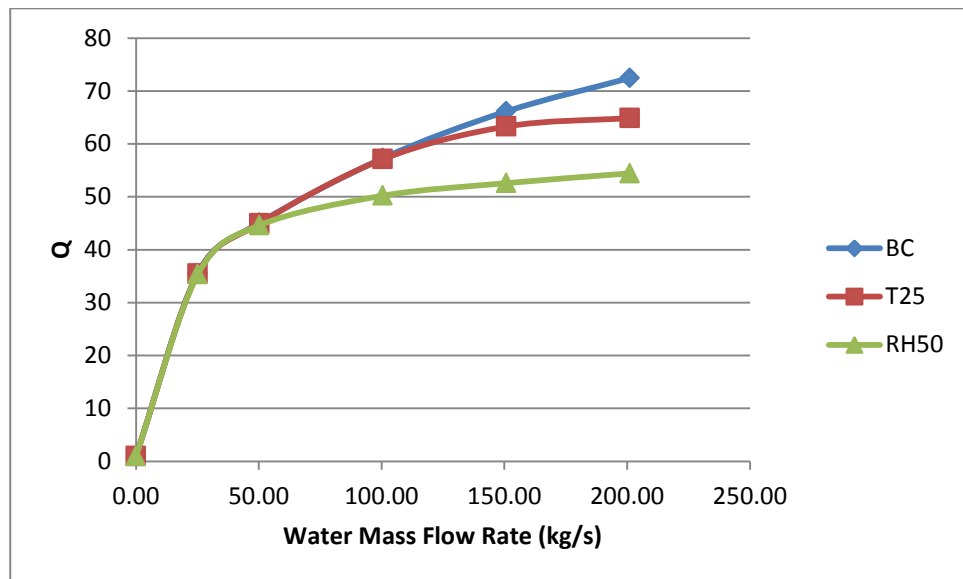


Figure 50. Tower 400x160- Density vs. Injection Rate

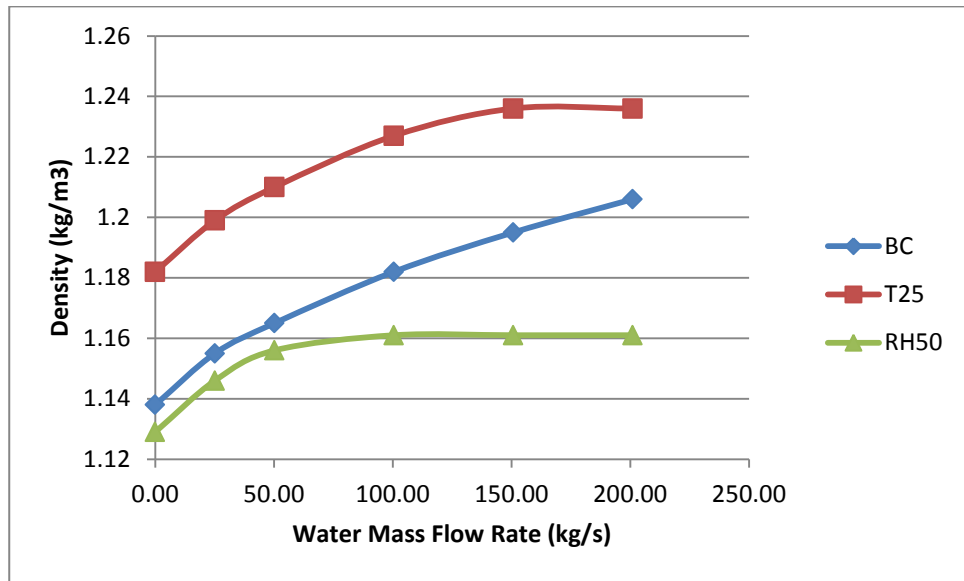


Figure 51. Tower 400x160- Velocity vs. Injection Rate

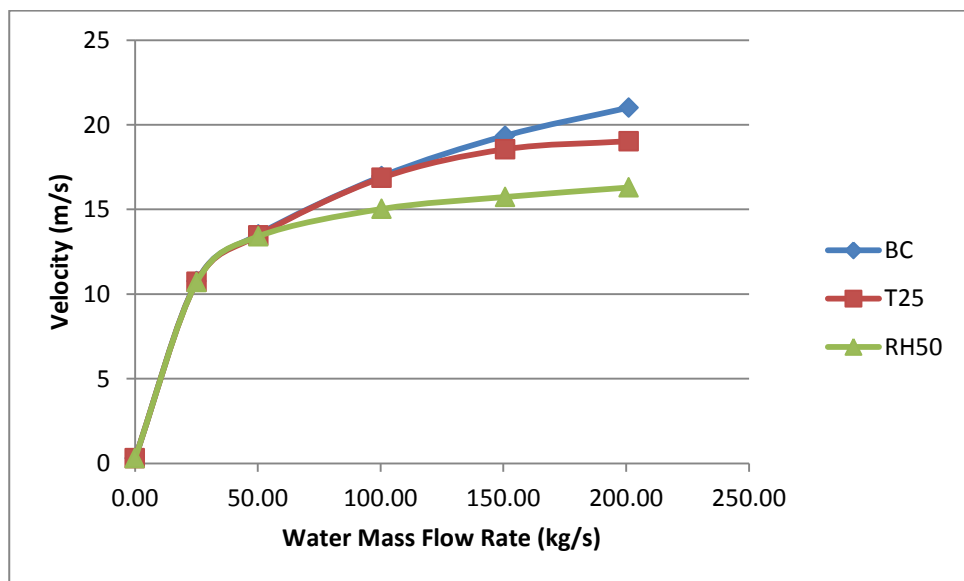


Figure 52. Tower 400x160- Temperature vs. Injection Rate

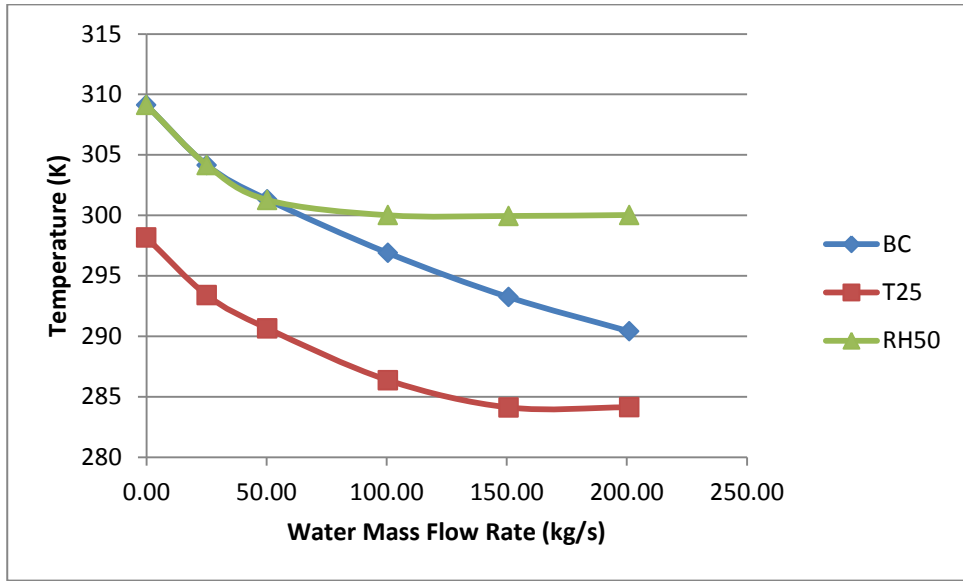
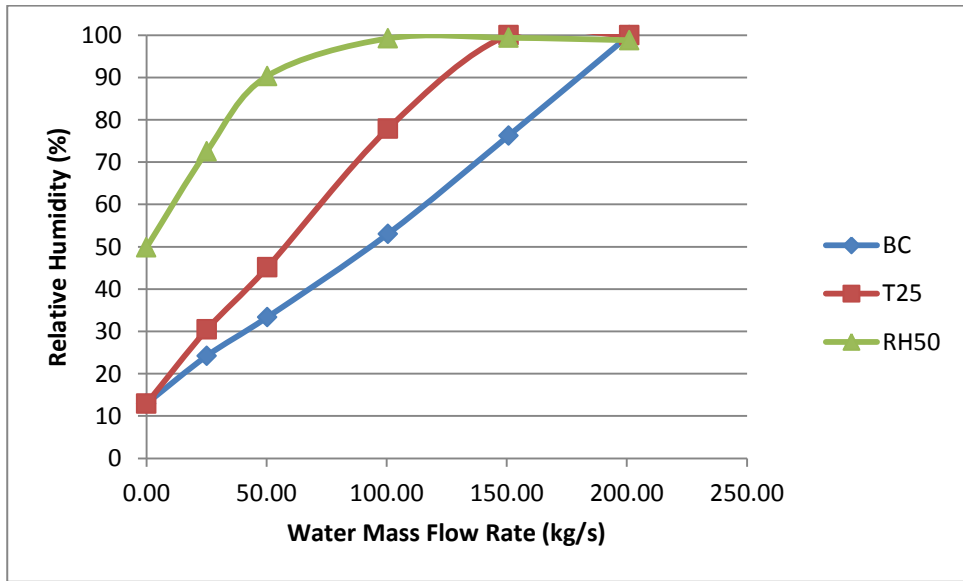


Figure 53. Tower 400x160- Relative Humidity vs. Injection Rate



7.3.2. Impact of Droplet Diameter

While investigating the droplet diameter, the injection rate for all cases was fixed at 50.27kg/s. Results show similar behavior to a 100m tower.

Figure 54. Tower 400x160- Q vs. Droplet Diameter

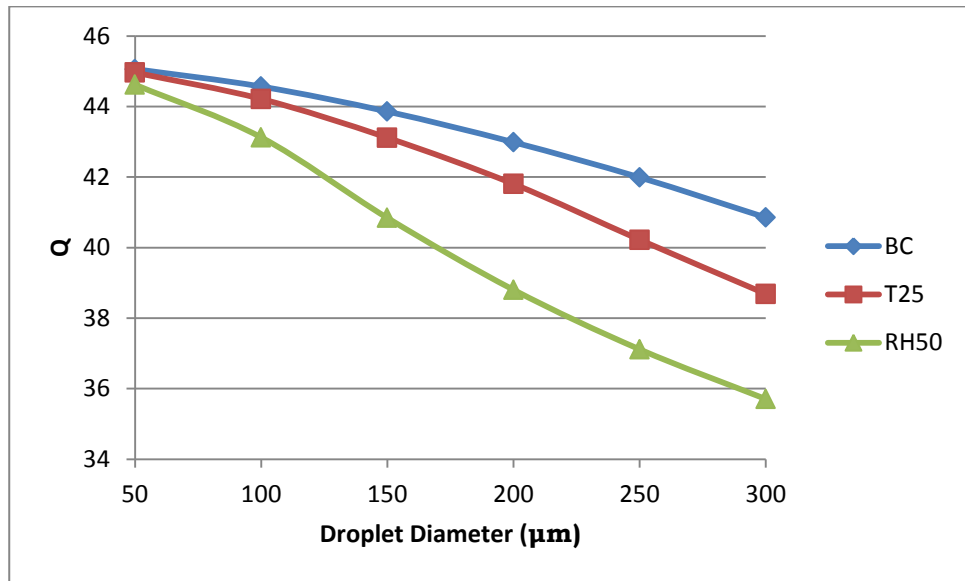


Figure 55. Tower 400x160- Density vs. Droplet Diameter

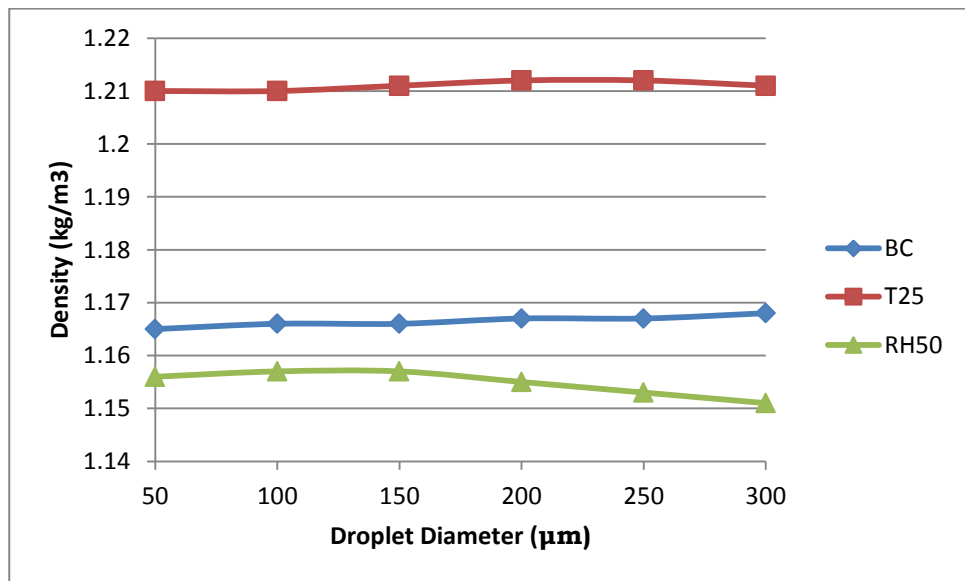


Figure 56. Tower 400x160- Velocity vs. Droplet Diameter

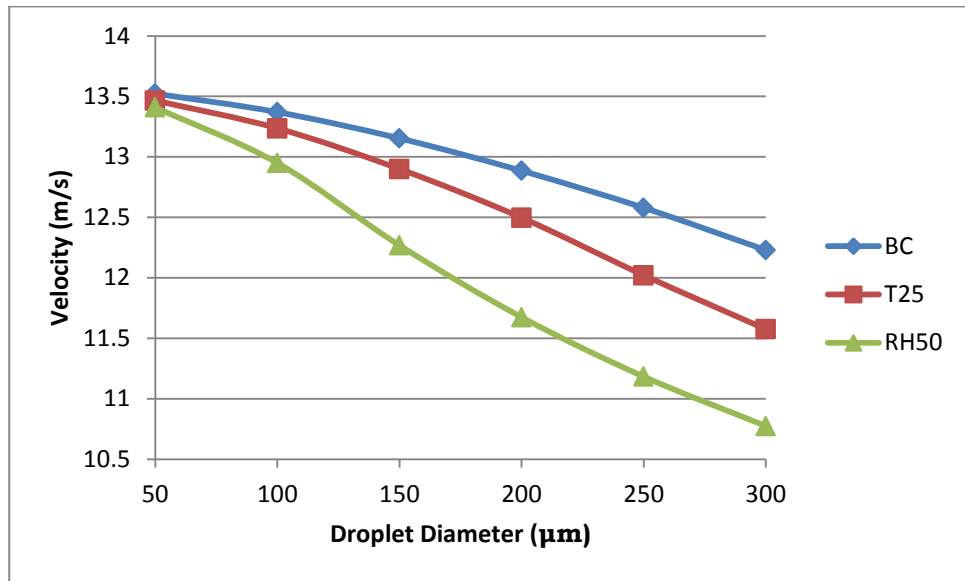


Figure 57. Tower 400x160- Temperature vs. Droplet Diameter

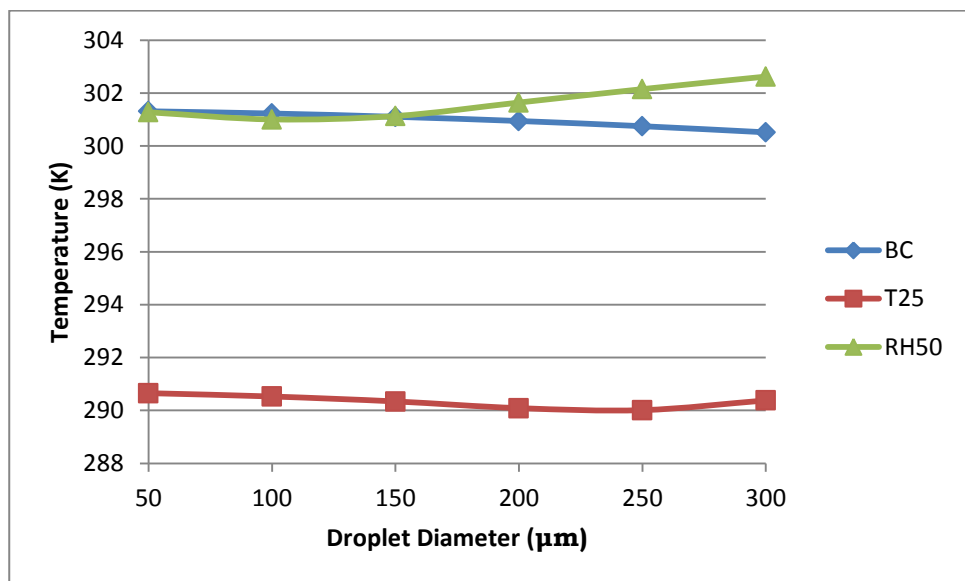
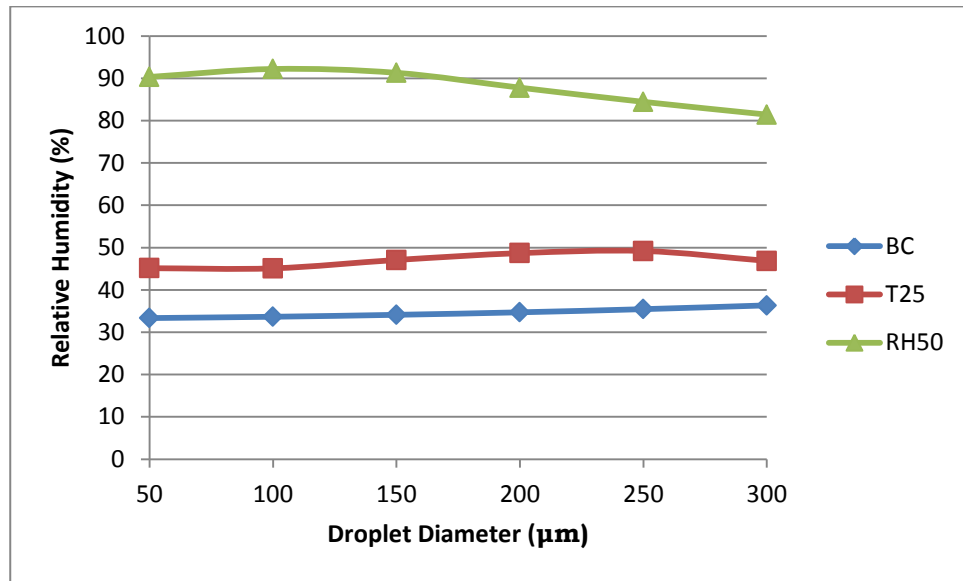


Figure 58. Tower 400x160- Relative Humidity vs. Droplet Diameter



7.3.3. Impact of Tower Height to Diameter Ratio

To study the impact of Height to Diameter ratio, the height of the tower is fixed at 400m. Three cases were considered, displayed in table 8.

Table 8. Impact of Tower Diameter- Cases

Tower Height (m)	Height to Diameter Ratio (H/D)	Tower Diameter (m)
400	2.5	160
400	1.5	267
400	3.5	115

From Figures 66 to 70, when the tower diameter decreases, terminal velocity increases since the inlet surface area decreases. Accordingly, the quantity of mass that is entrained from the environment is more.

Saturation conditions are achieved for an injection rate of 150kg/s for a diameter of 115m, 201 kg/s for a diameter of 160m and 352kg/s for a diameter of 267m. This is because as the total volume of the tower increases, more water is needed to saturate the air inside. Therefore, over these injection rates we can witness achieving temperature lows and density highs. Once saturation conditions are achieved, the exit conditions for temperature and density are the same regardless of diameter, and this is because the only factor which is different is total volume, so when the volume is more, we need more water to reach terminal conditions and vice versa for a lesser volume tower.

Figure 59. Impact of Tower H/D Ratio- Q vs/ Injection Rate

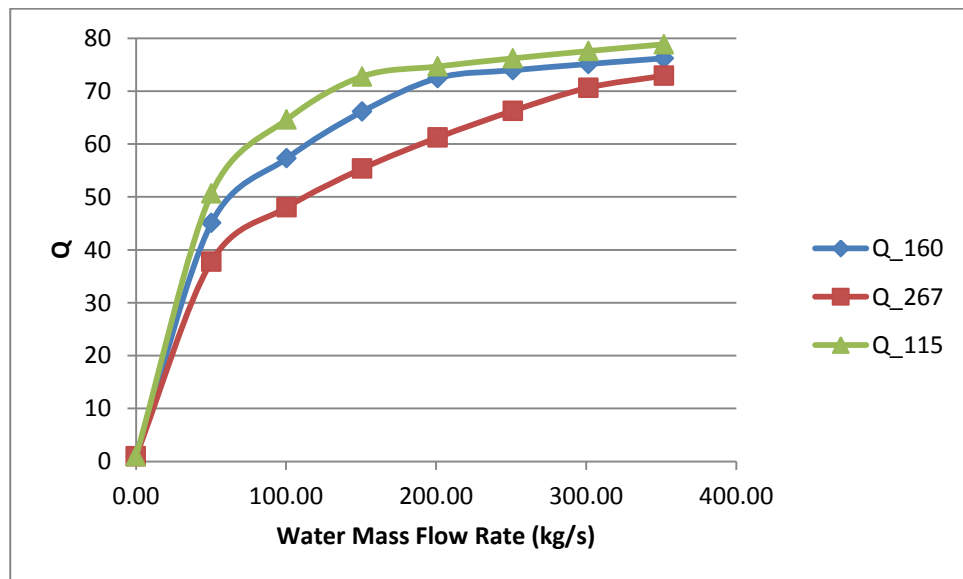


Figure 60. Impact of Tower H/D Ratio- Density vs/ Injection Rate

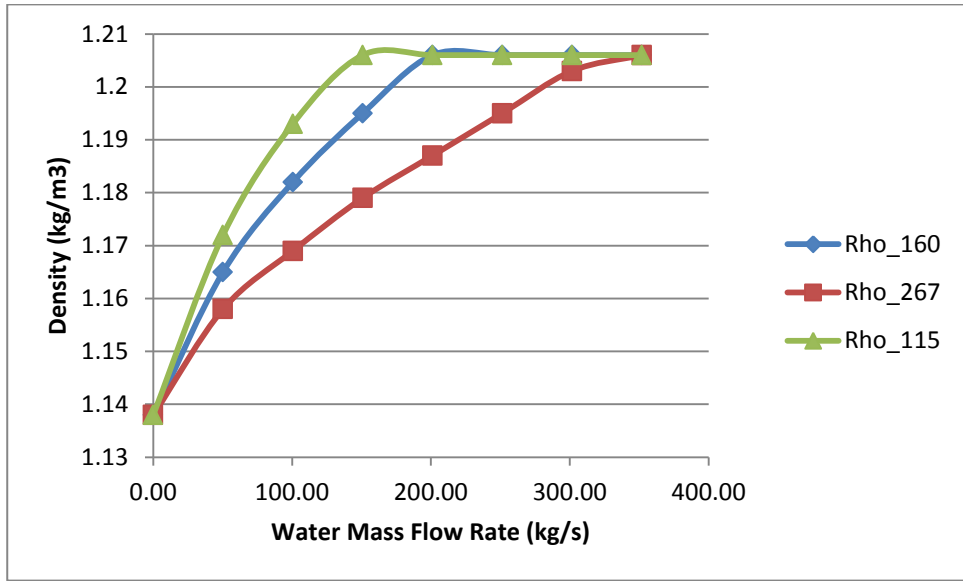


Figure 61. Impact of Tower H/D Ratio- Velocity vs/ Injection Rate

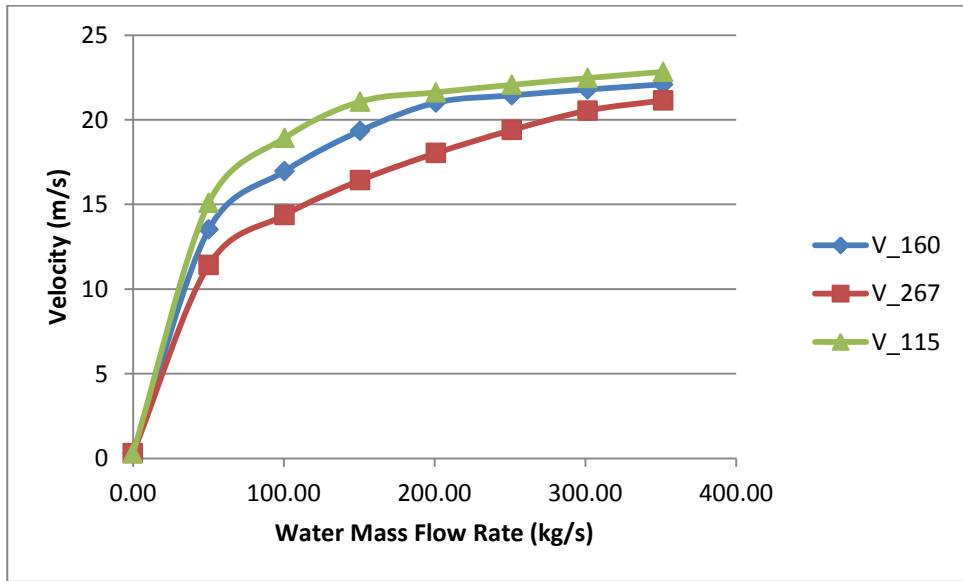


Figure 62. Impact of Tower H/D Ratio-Temperature vs/ Injection Rate

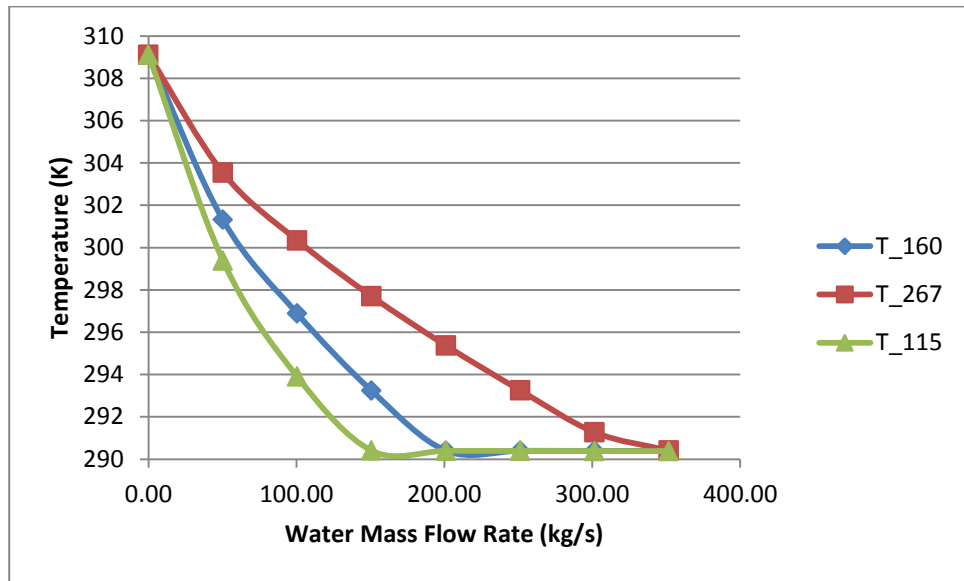
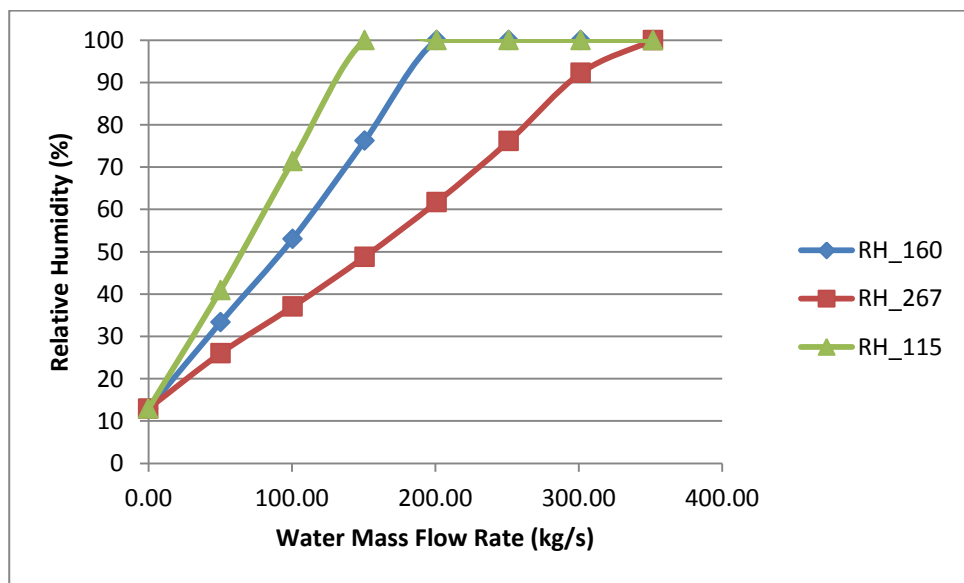


Figure 63. Impact of Tower H/D Ratio-Relative Humidity vs/ Injection Rate



7.4. Test Series V – 1000m Tower

7.4.1. Impact of Water Mass Flow Rate

For a tower of 1000m and diameter 400m, Figures 71 to 75 display exit conditions when varying water mass flow rate until saturation is achieved. Similar to all tower heights, exit conditions for temperature and density at saturation remain the same. Over 1000m, the maximum terminal velocity that can be achieved is 33.2 m/s for the base case, 30.1 m/s for an external temperature of 25°C, and 25.6 m/s when the outdoor relative humidity is 50%. In order to achieve these target results a water quantity of 754kg/s is required.

Figure 64. Tower 1000x400- Q vs. Injection Rate

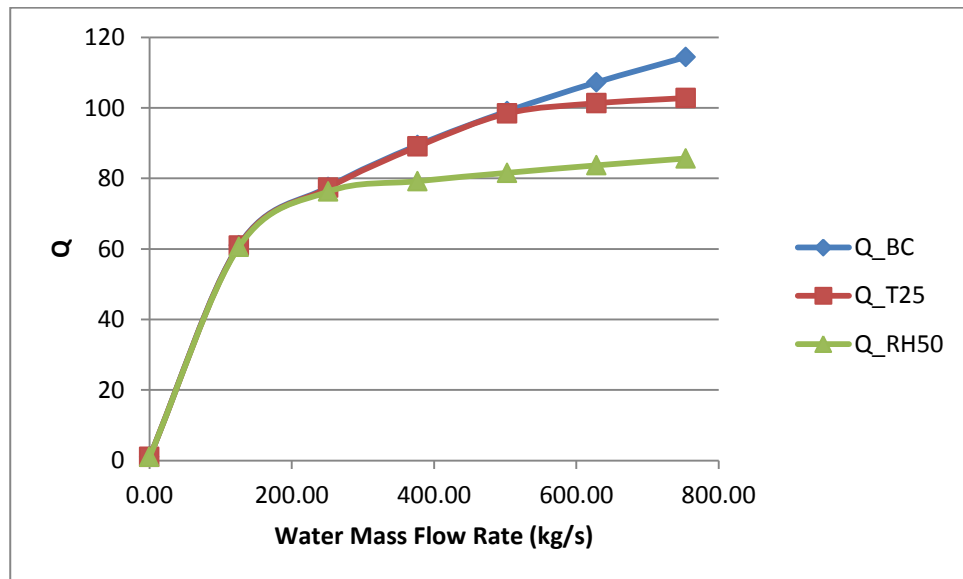


Figure 65. Tower 1000x400- Density vs. Injection Rate

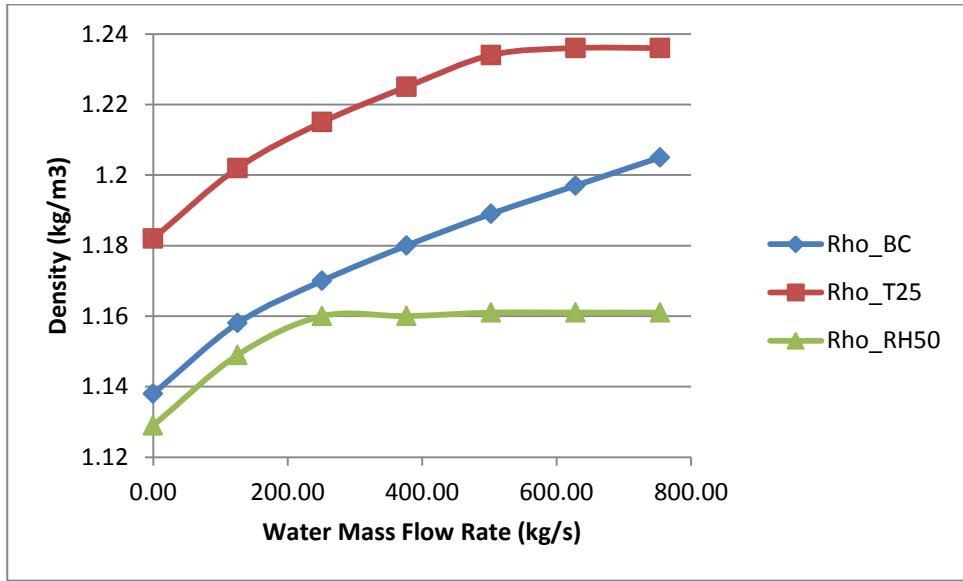


Figure 66. Tower 1000x400- Velocity vs. Injection Rate

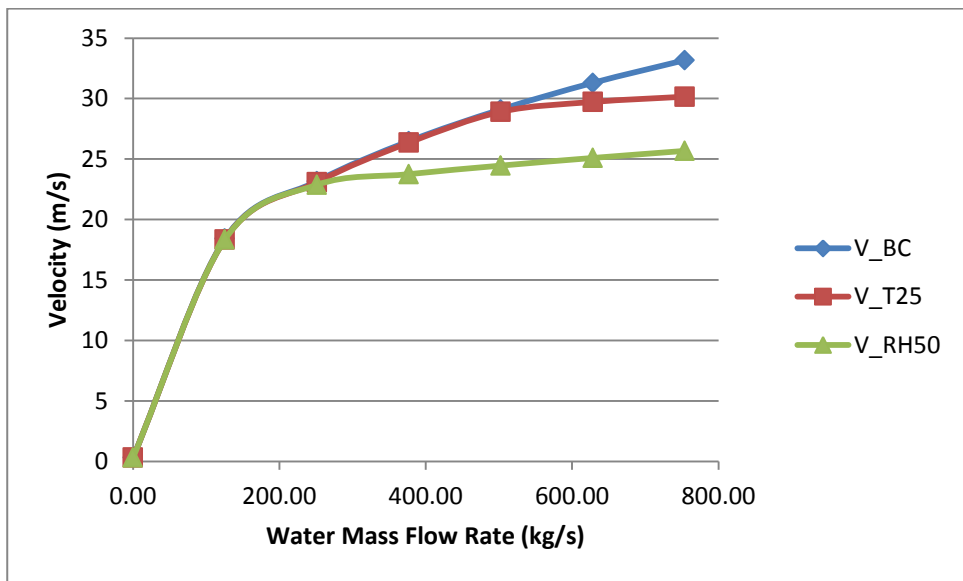


Figure 67. Tower 1000x400- Temperature vs. Injection Rate

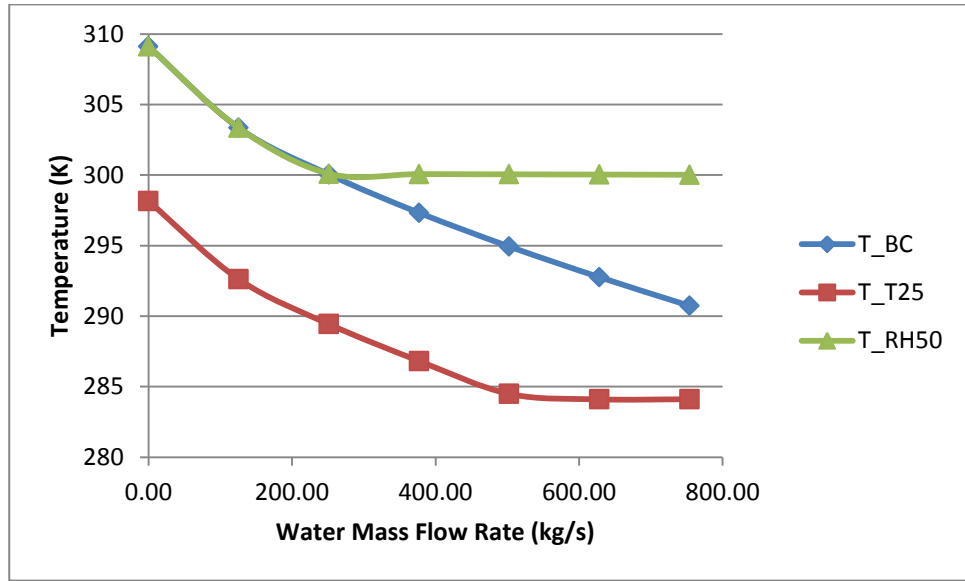
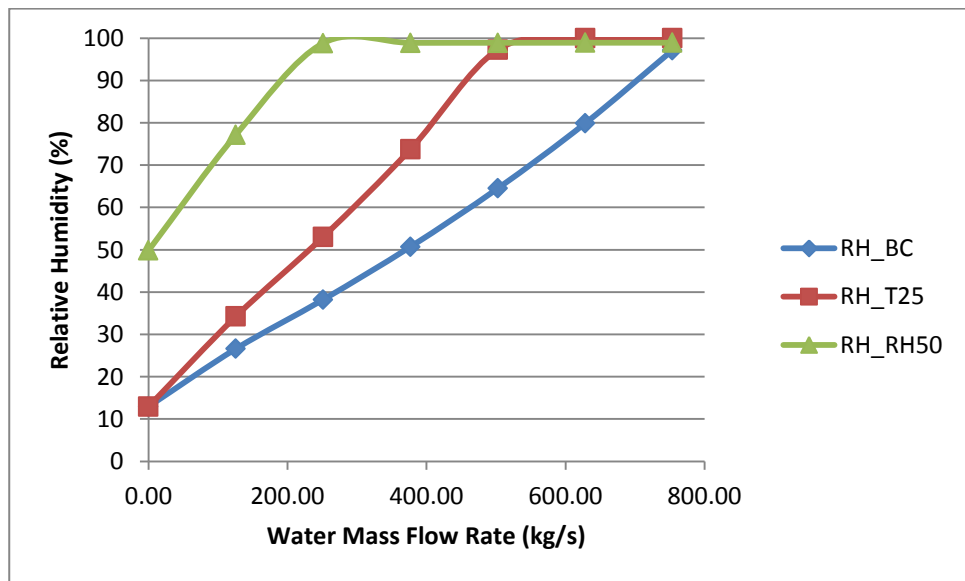


Figure 68. Tower 1000x400- Relative Humidity vs. Injection Rate



7.4.2. Impact of Droplet Diameter

Under this condition, the droplet diameter that induces the largest temperature drop differs for different tower heights. For instance, for a 100m tower, the lowest temperature was obtained over a droplet diameter of 150 μ m, whereas over 400m, the

lowest temperature was obtained over a droplet diameter of 250 μm . Table 8 below shows the droplet diameter for each case which induces the lowest temperature per tower height. As the tower height increases, the droplet diameter which induces the largest temperature drop increases. This is because the droplet has more room to gain additional heat from the environment before it evaporates completely or escapes the domain. For the case where the outdoor relative humidity is 50%, the case is different as the conditions are near saturation.

Table 9. Droplet Diameter which Induces Largest Temperature Drop

	BC	T25	RH50
20 m Tower	100 μm	100 μm	50 μm
100m Tower	200 μm	150 μm	100 μm
400m Tower	300 μm	250 μm	100 μm
1000m Tower	300 μm	250 μm	50 μm

For illustration, Figures 76 to 80 show exit conditions of the three representative cases while varying droplet diameter.

Figure 69. Tower 1000x400- Q vs. Droplet Diameter

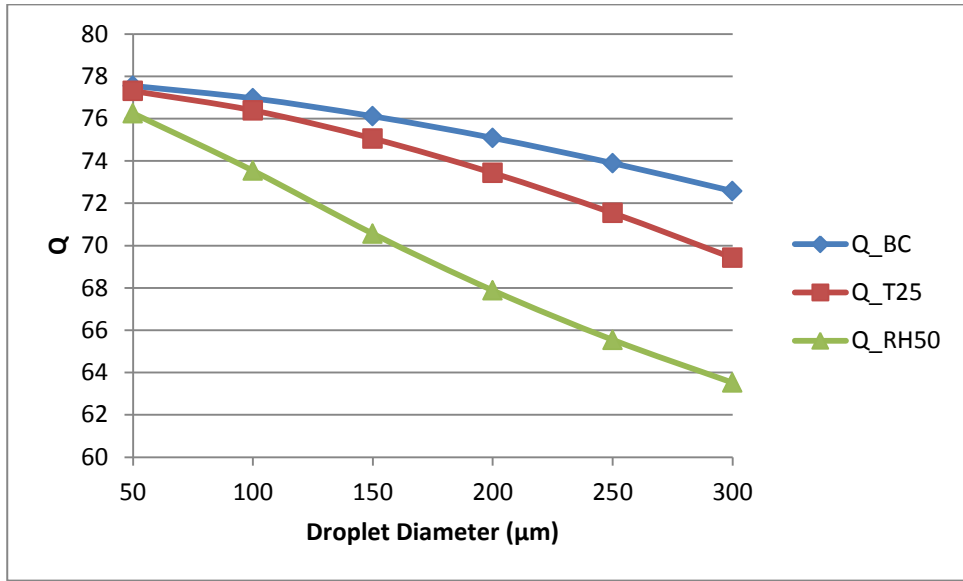


Figure 70. Tower 1000x400- Density vs. Droplet Diameter

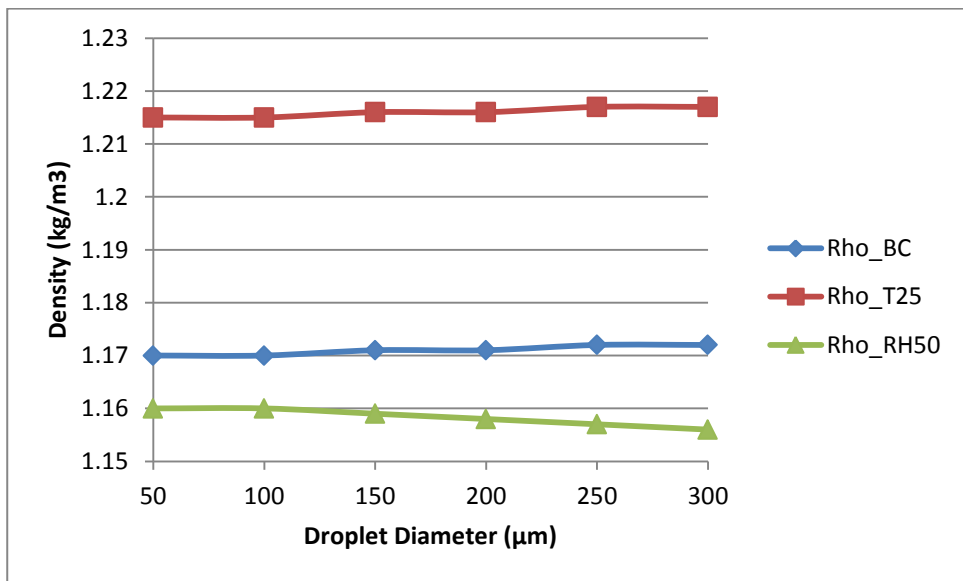


Figure 71. Tower 1000x400- Velocity vs. Droplet Diameter

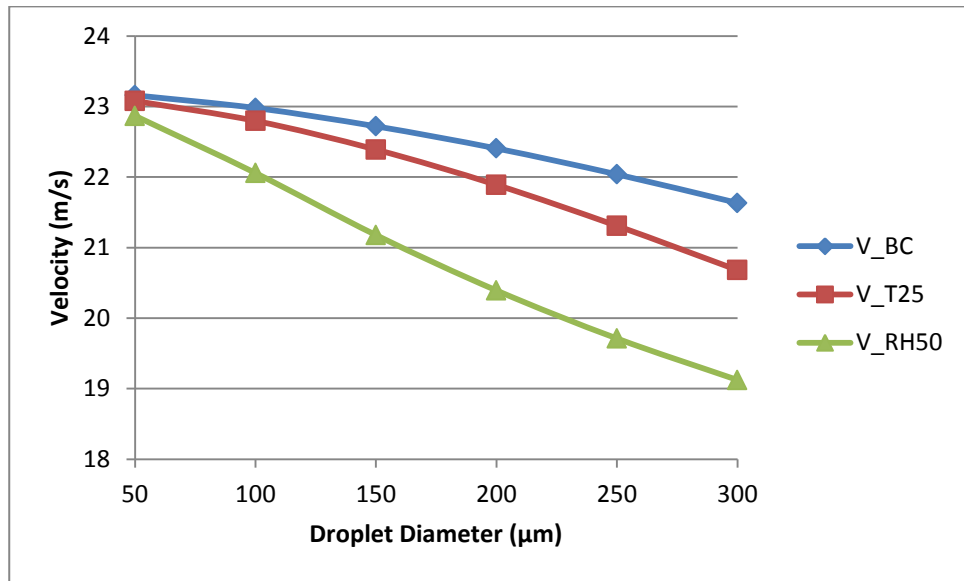


Figure 72. Tower 1000x400- Temperature vs. Droplet Diameter

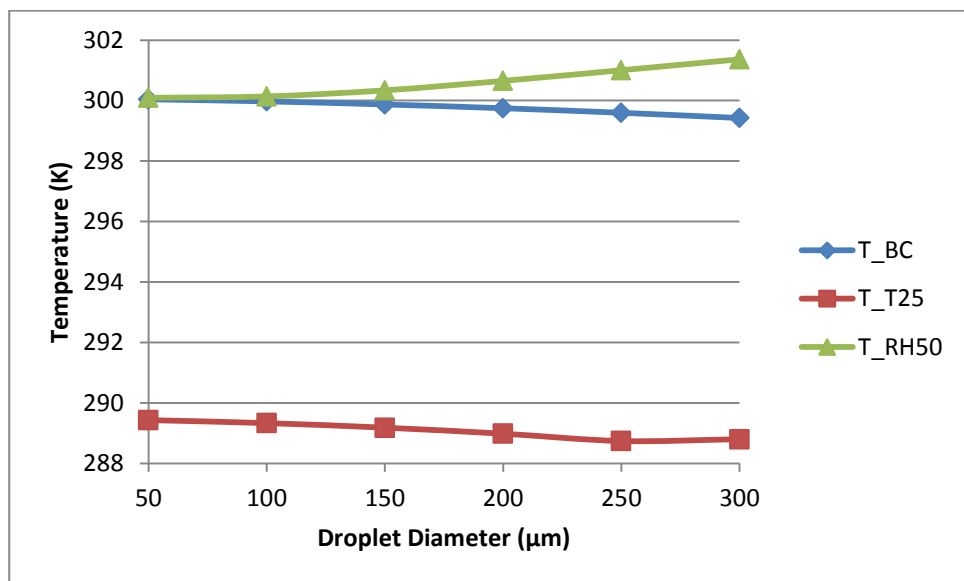
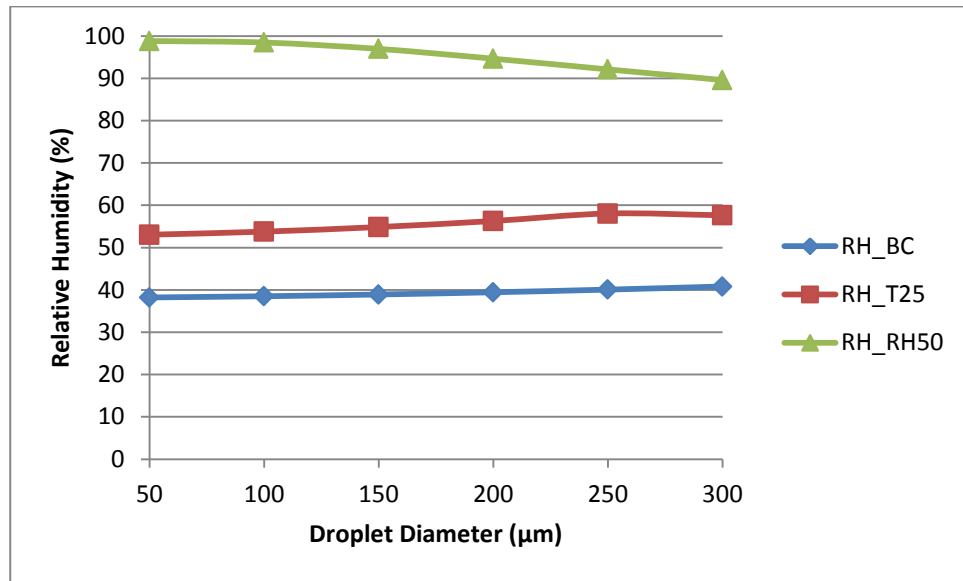


Figure 73. Tower 1000x400- Relative Humidity vs. Droplet Diameter



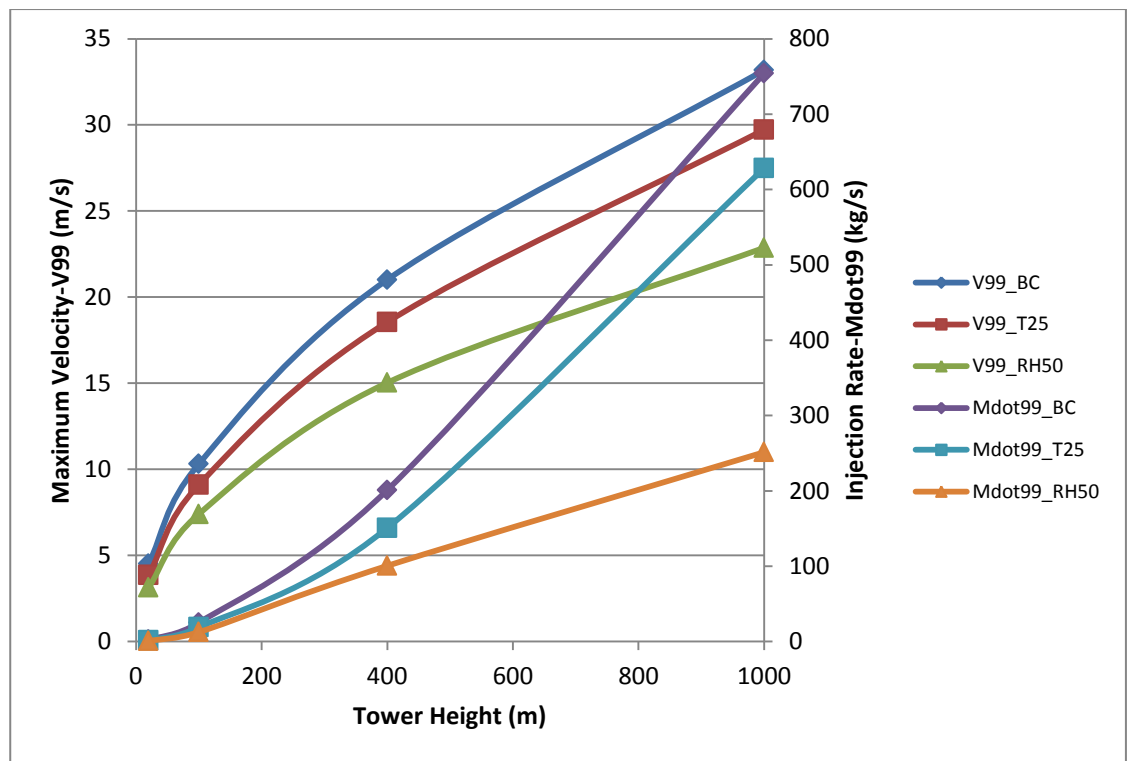
7.5. High Level Summary

In this work, simulations have been conducted over variable tower heights with a height to width ratio of 2.5 in order to predict exit conditions. It has been shown that as the height of the tower increases, more wind can be entrained into the tower from the environment. Let V_{99} and $Mdot_{99}$ respectively represent the velocity and injection rates when a 99% relative humidity is achieved at outlet. Figure 74 shows the achievable terminal velocity as a function of tower height as well as the injection rate required to realize such conditions for each of the three representative cases. Velocity profiles are consistent with the power law with an R^2 value of 0.99, yet injection rate profiles vary with ambient conditions. For a 20m tower, injection requirements range from 0.94 kg/s to 2.51 kg/s which induce a terminal velocity ranging from 3.1m/s to 4.5m/s. Yet a high speed velocity airflow is required to drive turbines at the outlet and

this can be achieved with increasing the height of the tower whereby a terminal velocity of 33.1 m/s is achievable over 1000m.

In order to produce a high enough airflow speed, the tower must be at least 400m high, yet the water requirements become massive starting from 350kg/s over 400m, reaching up to 754kg/s over 1000m. Considering that enormous quantities of water are required to operate the system, an energy analysis is necessary to evaluate the net energy output to deem the economic value of constructing a tower.

Figure 74. V99 and Mdot99 vs. Tower Height



CHAPTER 8

CONCLUSION AND FUTURE WORK

A Solar Wind Energy Tower is ideally located in a hot and dry region and operates as an energy conversion device that generates electricity. Till date, no working prototype exists for an Energy Tower due to a massive investment required, in addition to the huge quantity of water required to operate the facility. In this research, a CFD model for an energy tower is produced that can evaluate performance within the effective domain of the tower as well as predict exit conditions given ambient conditions and spray characteristics. Simulations were conducted on a domain prior to diverting the airflow through smaller cross sections where the turbines are located in order to justify the need to construct a tower of 1000m rather than constructing a small scale tower with a spray system and diverting the airflow through narrower channels to obtain a high speed airflow. CFD simulations show that an exit velocity of 33.1 m/s can be achieved solely by the evaporation process without any geometry manipulation. Future works may introduce the full tower geometry including the curved flare at the top of the tower, a cone like structure at the bottom to divert the airflow into channels where wind turbines are located.

This research was intended to present a design tool for an Energy Tower in order to identify water requirements and evaluate exit conditions as well as understand heat and mass transfer phenomena through simulation. An additional value of this research is employing a full buoyancy model, which has not been incorporated in previous studies of energy towers with spray systems. This model predicts the

buoyancy force more accurately than boussinesq's approximation. In addition, density of humid air was considered.

Parametric studies show that increasing tower height and diameter lead to the increase in velocity that can be attained at the outlet. Injecting water beyond saturation conditions has little effect on the final velocity, yet the velocity does increase mildly as the weight of additional droplets contribute to enhancing the downdraft. Increasing droplet size decreases the final velocity that can be attained, yet injecting droplets less than 100 μm is claimed to be energy expensive.

Future work may couple the results presented in this research with an energy model to study the optimum configuration that maximizes energy output at minimum cost. Additional future work may also entail comparison between FLUENT and open-source CFD codes such as OPENFOAM. Results also reveal that Energy Towers do not necessarily need to be located in hot and dry regions. Regardless of whether it would be economical or not, the tower can also operate in cold dry regions or even warm climates.

REFERENCES

- [1] P. Carlson, 1974, "Power Generation through Controlled Convection (Aeroelectric Power Generation)," U.S. Patent 3,894,393 A.
- [2] D. Zaslavsky, R. Guetta, R. Hitron, G. Krivchenko, M. Burt, and M. Poreh, 2011, "Sharav Sluices Ltd Files Patent Application for Renewable Resource Hydro/Aero-power Generation Plant and Method of Generating Hydro/Aero-power," U.S. Patent 6,510,687 B1.
- [3] P. Zhang and C.K. Law, 2007, "Theory of Bouncing and Coalescence in Droplet Collision," G16, 5th US Combustion Meeting, San Diego.
- [4] S. Hassid, I. Merksamer, and R. Guetta, 2012, "Energy Towers- The Effect of Droplet Coalescence on Power and the Environment," *Solar Energy*, **86**, pp. 1443-1453.
- [5] S. Subramaniam, 2013, "Lagrangian-Eulerian Methods for Multiphase Flows," *Progress in Energy and Combustion Science*, **39**, pp. 215-245.
- [6] D. Kang and R. K. Strand, 2013, "Modeling of Simultaneous Heat and Mass Transfer within Passive Down-draft Evaporative Cooling (PDEC) Towers with Spray in FLUENT," *Energy and Buildings*, **62**, pp. 196-209.
- [7] V. Kalantar, 2009, "Numerical Simulation of Cooling Performance of Wind Tower (Baud-Geer) in Hot and Arid Region," *Renewable Energy*, **34**, pp. 246-254.

[8] M.J. Cook, D. Robinson, K.J. Lomas, 2000, N.T. Bowman, and H. Eppel, "Passive Downdraught Evaporative Cooling: II. Airflow Modelling," *Indoor and Built Environment*, **9**, pp. 325-334.

[9] E. Omer, R. Guetta, I. Ioslovich, P. Gutman, and M. Borshchevsky, 2008, "Optimal Design of an Energy Tower Power Plant," *IEEE Trans. on Energy Conversion*, **23**, pp. 215-225

[10] G. Abhinava, N. Swarnkar, S. Behera, and G. Edison, "Creation of Artificial Downdraft for Wind Power Plant," *International Conference on Energy Efficient Technologies for Sustainability*, 2013, pp. 571-576.

[11] J.C. Kloppers and D.G. Kroger, 2005, "The Lewis Factor and its Influence on The Performance Prediction of Wet-Cooling Towers," *International Journal of Thermal Sciences*, **44**, pp. 879-884.

[12] S.K. Shukla, P. Shukla, and P. Ghosh, 2011, "Evaluation of Numerical Schemes for Dispersed Phase Modeling of Cyclone Separators," *Engineering Applications of Computational Fluid Mechanics*, **5**, pp. 235-246.

[13] M.F. El Amin, S. Sun, and W. Heidemann, 2010, "Analysis of a Turbulent Buoyant Confined Jet Modeled using Realizable $k-\varepsilon$ Model," *Heat Mass Transfer*, **46**, pp. 943-960.

[14] ASHRAE, "2001 ASHRAE FUNDAMENTALS HANDBOOK (SI)," Amer Soc of Heating, Refrigerating & A-C Engineers, 2001, ch. 6.

[15] R. Belarbi, C. Ghiaus, and F. Allard, 2006, "Modeling of Water Spray Evaporation: Application to Passive Cooling of Buildings," *Solar Energy*, **80**, pp. 1540-1552.